ESD-TR-80-197

LEVEL II



# Project Report

RST-5

L. H. Johnson

## The Shift and Scale Invariant Fourier-Mellin Transform for Radar Applications

14 October 1980

Prepared for the Department of the Navy
under Electronic Systems Division Contract F19628-80-C-0002 by

**Lincoln Laboratory**

MASSACHUSETTS INSTITUTE OF TECHNOLOGY

*LEXINGTON, MASSACHUSETTS*

The work reported in this document was performed at Lincoln Laboratory, a center for research operated by Massachusetts Institute of Technology. The work was sponsored by the Department of the Navy under Air Force Contract F19628-80-C-0002.





This technical report has been reviewed and is approved for publication.

FOR THE COMMANDER

Joseph C. Sylek

Joseph C. Sylek
Project Officer
Lincoln Laboratory Project Office

MASSACHUSETTS INSTITUTE OF TECHNOLOGY
LINCOLN LABORATORY

# THE SHIFT AND SCALE INVARIANT FOURIER-MELLIN TRANSFORM FOR RADAR APPLICATIONS

*L. H. JOHNSON*
*Group 37*

PROJECT REPORT RST-5

14 OCTOBER 1980



LEXINGTON MASSACHUSETTS

## ABSTRACT

Automatic classification of targets viewed by radar is complicated by variations in target aspect relative to the radar line-of-sight (RLOS). This report investigates the possibility of reducing the effects of target aspect by using the scale invariance of the Mellin transform. The properties of the Mellin transform are developed in analogy with the Fourier transform and illustrated using simple test functions and digitally implemented transforms. Simulated radar ship profiles demonstrate that a change in aspect is not equivalent to a change in target scale for realistic targets, however. Automatic classification results, for both simulated and actual radar ship profiles, confirm that using a combination Fourier-Mellin transform for feature selection appears at best comparable to the results obtained using the Fourier transform alone for feature selection.

TABLE OF CONTENTS

## LIST OF ILLUSTRATIONS



## LIST OF TABLES

# 1. INTRODUCTION

Identification of targets is a significant problem facing the defense community. Current weapon systems are capable of engaging targets at ranges far in excess of those as which the targets may be identified. Amelioration of the problem through the application of long range sensors and the development of identification techniques is being actively pursued.

This report is concerned with automatic classification of ship targets sensed by radar. In particular, it is one attempt to address the difficulties encountered when the relative aspect is varied between a ship and the radar line-of-sight (RLOS). This is done by considering a scale invariant Mellin transform applied as a feature selector for automatic ship classification.

Figure 1 shows schematically the general pattern recognition process. Data provided by sensors is preferentially selected or otherwise manipulated by a feature selection technique. The selected features are then combined with other knowledge and used to make a decision as to the most representative class. The class decision is the identification desired.

Radar cross section (RCS) vs range profiles of ships have been provided by the Naval Weapons Center, China Lake, California. Averaged profiles are available at approximately one degree aspect increments. This data is divided into training and testing sets. The training set is used to train a classifier while the testing set tests its performance. Both data subsets pass through the same feature selection process.

Automatic classification of a target into one of several possible classes is complicated by allowing the viewing aspect to vary. This is due to induced variations in the perception of that target. For one dimensional targets, changing the viewing aspect is equivalent to scaling of the length by the cosine of the aspect angle. Three-dimensional targets behave

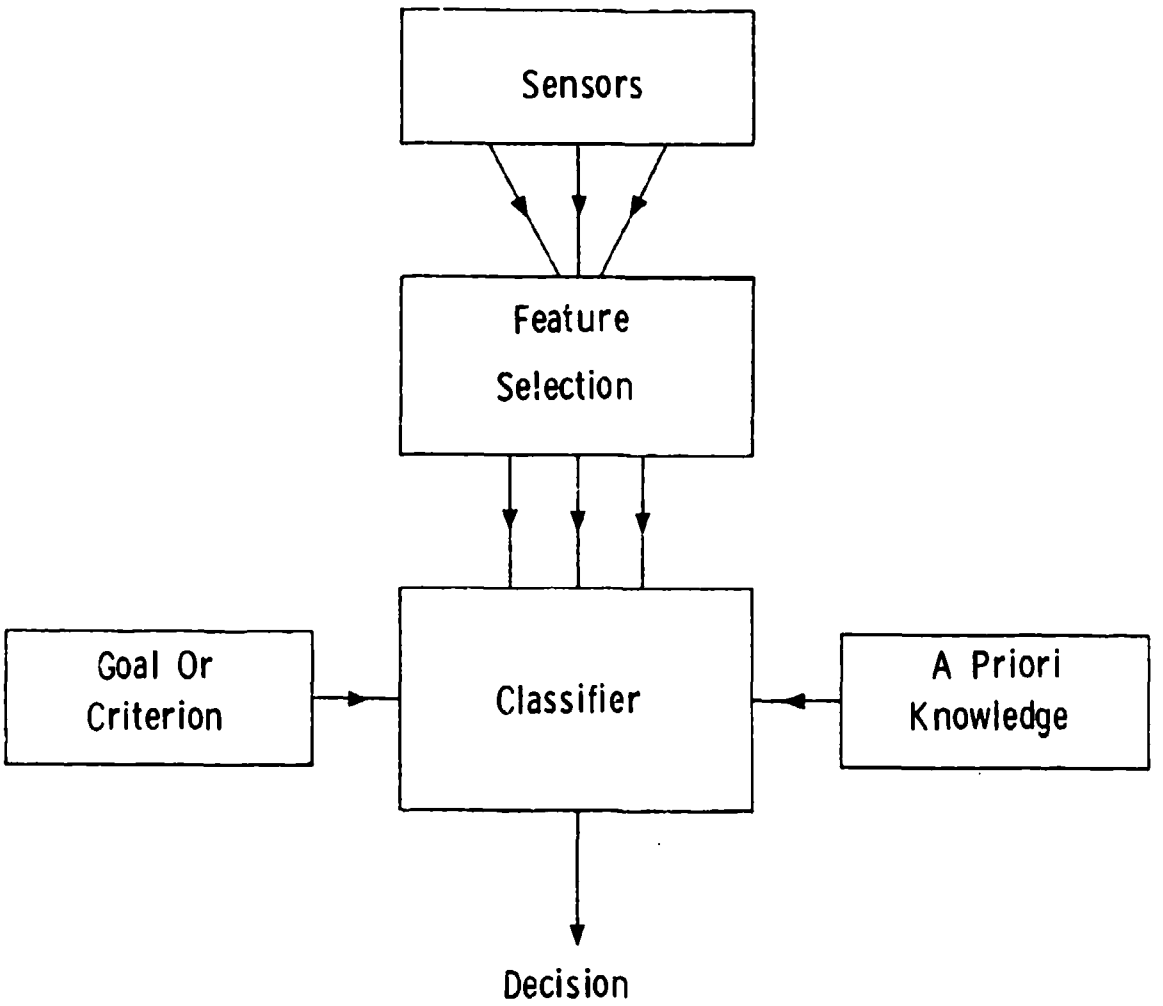


Fig. 1. The pattern recognition process

in a more complicated manner since typically only a two dimensional projection is available. In this case, besides being scaled, portions of a target may appear or disappear.

A possible solution to this problem is to construct a large number of projections of training targets at many different aspects. Classification may then be performed by comparing a test target with all projections. The class of the projection with the "closest" match could be taken as the class to which the test target is assigned.

An alternative solution, at least for one dimensional targets, is to perform a transformation of a target to a new space which is independent of viewing aspect. Target classes must remain distinct, of course. Classification should now be considerably easier since aspect complications are removed. The transformation would be most useful if no a priori knowledge of aspect angle is required.

This second approach is investigated in this report using the mathematical operation known as the Mellin transform. The transform has the desirable property that its magnitude is invariant under scaling of the function which is being transformed. This is analagous to the invariance of the Fourier transform under translation. The scale invariance of the Mellin transform should completely remove aspect angle dependence for one dimensional targets with multiple scattering and interference excluded. However, only approximate scale invariance can be expected for three dimensional targets.

A combination Fourier and Mellin transform can also be considered. This Fourier-Mellin transform should be invariant under both shift and scale operations. The utility of the Fourier-Mellin transform as a feature selector is judged by comparing its classification performance with that of a classifier using only the Fourier transform for feature selection.

In the following sections the Mellin transform and some of its properties are presented. In all cases comparisons with the Fourier transform are made. Transforms of simple test functions are presented next to illustrate the operation of the transforms. Fourier-Mellin transforms of simulated radar ship profiles are then investigated. These profiles emphasize that for realistic targets a change in aspect is not equivalent to a change in scale. Finally automatic classification results are compared for two cases using either the Fourier-Mellin transform or the Fourier transform for feature selection. Both simulated and actual radar ship profiles are used.

Throughout the report emphasis is not on the formal mathematical properties of the Mellin transform. Instead the emphasis is on digital implementation and insight into the physical operation of the transform.

## 2. MELLIN TRANSFORM

Mellin transforms are discussed in many books dealing with mathematical transforms.[1,2] The usual definition is

$$M(s) = \int_0^\infty f(x) x^{s-1} dx \tag{1}$$

where $s=\sigma+i\tau$. Here, the real part of s, $\sigma$, is chosen to be a constant whose value is partially determined by the function $f(x)$ such that the integral converges. The imaginary part of s, $\tau$, is the transform variable.

The scale invariance of the Mellin transform is easily shown by considering a function $f(ax)$. Then

$$M(s,a) = \int_0^\infty f(ax) x^{s-1} dx = a^{-s} M(s) \tag{2}$$

In a similar way the Fourier transform

$$F(\nu) = \int_{-\infty}^\infty f(x) e^{-i2\pi\nu x} dx \tag{3}$$

can be shown to be shift or translation invariant by considering $f(x-a)$

$$F(\nu,a) = \int_{-\infty}^\infty f(x-a) e^{-i2\pi\nu x} dx = e^{-i2\pi\nu a} F(\nu) \tag{4}$$

Clearly, for the Fourier transform under translation

$$|F(\nu,a)| = |F(\nu)| \tag{5}$$

while for the Mellin transform under scale

$$|M(s,a)| = a^{-\sigma} |M(s)| \tag{6}$$

In general there is a multiplicative factor relating the two Mellin transforms. When comparing two Mellin transforms, this factor is easily removed by normalization. On the other hand, the multiplicative factor may be used directly to find the relative scale between the two functions. Consider now the Fourier transform of a function f(ax-b).

$$F(\nu,a,b) = \int_{-\infty}^{\infty} f(ax-b)e^{-i2\pi\nu x}dx \tag{7}$$

Letting y=ax-b this becomes

$$\begin{aligned} F(\nu,a,b) &= \frac{1}{|a|}e^{-i2\pi\frac{\nu}{a}b}\int_{-\infty}^{\infty} f(y)e^{-i2\pi\frac{\nu}{a}y}dy \\ &= \frac{1}{|a|}e^{-i2\pi\frac{\nu}{a}b}\ F(\tfrac{\nu}{a}) \end{aligned} \tag{8}$$

Finding the absolute magnitude

$$\left|F(\nu,a,b)\right| = \frac{1}{|a|}\left|F(\tfrac{\nu}{a})\right| \tag{9}$$

Note that in addition to the multiplicative factor 1/a, the frequency, $\nu$, has also been scaled by 1/a. The Mellin transform should be capable of removing the scale dependence.

Thus consider the Mellin transform of Eq. (9) with a>o

$$M_F(s,a) = \int_0^{\infty}\frac{1}{a}\ |F(\tfrac{\nu}{a})|\ \nu^{s-1}d\nu = a^{s-1}\ M_F(s) \tag{10}$$

$$|M_F(s,a)| = a^{\sigma-1}\ |M_F(s)| \tag{11}$$

This Fourier-Mellin transform is independent of the position b of f(ax-b) (translation invariant) and except for a multiplicative factor is independent of the scale a of f (scale invariant). Indeed, if $\sigma$ can be chosen equal to 1, the multiplicative factor also disappears.

Unfortunately, each time the magnitude of one of the transforms is taken, all phase information present in that transform is lost. An important question is then whether sufficient information remains from the two successive transforms to make this Fourier-Mellin transform useful.

Two other facts concerning the Mellin transform are its relation to the Fourier transform and the inverse Mellin transform. Equation (1) can be rewritten as

$$M(s) = \int_{\infty}^{\infty} \left[ f(x) x^{\sigma-1} \right] e^{i\tau \log x} \, dx \tag{12}$$

This form is similar to the Fourier transform in Eq. (3). The argument of the phase factor is now a nonlinear function of x, however. Also notice that the range of integration for the Mellin transform is only over non-negative x.

The Mellin transform can be converted to a Fourier transform by making a change of variable

$$x = e^{y} \tag{13}$$

Then

$$M(s) = \int_{-\infty}^{\infty} \left[ f(e^{y}) e^{\sigma y} \right] e^{i\tau y} \, dy \tag{14}$$

This is a Fourier transform of the distorted function $f(e^{y})$ weighted by $e^{\sigma y}$. Equation (14) is particularly important in implementing the Mellin transform. This is discussed more fully in the next section.

Further insight into the effects produced by tne application of Fourier or Mellin transforms can be gained by considering the inverse transforms.

$$F^{-1}(x) = \int_{-\infty}^{\infty} g(\nu) e^{i2\pi\nu x} d\nu \tag{15}$$

$$M^{-1}(x) = \frac{1}{2\pi i} \int_{\sigma-i\infty}^{\sigma+i\infty} g(s) x^{-s} ds \tag{16}$$

The utility of these transform pairs becomes apparent when the effects of filtering in the transform variable (frequency) domain are investigated. A resultant filtered function produced by a forward transform, multiplication by a filter function, and an inverse transform back to the space domain may be easily compared to the original, unfiltered function. Note that in this procedure the transform phase information is not discarded. This implies that in the case of the combined Fourier-Mellin transform as defined above it is not possible to return to the original input function. This is due to removal of the Fourier phase information before the Mellin transform is performed.

Finally, a function and its Fourier transform satisfy Parseval's theorem.

$$\int_{-\infty}^{\infty} |f(x)|^2 \, dx = \int_{-\infty}^{\infty} |F(\nu)|^2 \, d\nu \tag{17}$$

A similar relation may be found for the Mellin transform.

$$\int_{-\infty}^{\infty} |f(x)|^2 \, x^{2\sigma-1} dx = \int_{-\infty}^{\infty} |M(\nu)|^2 \, d\nu \qquad \tau = 2\pi\nu \tag{18}$$

These relations may be useful when transform coefficients are used as components of feature vectors in pattern recognition techniques. Since the dimension of the feature vectors may be much less than the number of transform coefficients available, Eq. (17) or (18) may give a relative approximation to the amount of information retained in the feature vectors.

## 3. MELLIN TRANSFORM IMPLEMENTATION

The Mellin transform can be implemented in several ways. The ability of lenses to perform Fourier transforms implies that the Mellin transform can also be performed optically by making use of Eq. (14). The requirement for processors of this type is to sample the input function at spacings $x=e^{y}$. Scale invariant optical Mellin transforms have been sucessfully performed (see Refs. {3} and {4}).

Mellin transforms can also be performed digitally. Suppose that a function f(x) is defined by values taken at equal increments, $\Delta x$.

$$f(x) = \{ f(j\Delta x) \quad j = 0,1,\ldots,N-1 \} \tag{19}$$

Then Eq. (1) becomes

$$M(s) \approx \sum_{j=0}^{N-1} f(j\Delta x)(j\Delta x)^{s-1}\Delta x \tag{20}$$

This form of the Mellin transform suffers from computation restrictions similar to those found in calculating the "slow" Fourier transform.

A better approach is to use the Fourier equivalent of the Mellin transform, Eq. (14). This integral is evaluated by summing contributions at equal increments in y. Rewriting Eq. (13)

$$x=\Delta x e^{j\Delta y} \tag{21}$$

Equation (14) becomes

$$M(\tau) \approx (\Delta x)^{\sigma+i\tau}\Delta y \sum_{j=-\infty}^{\infty} f(\Delta x e^{j\Delta y}) e^{j\sigma\Delta y} e^{ij\tau\Delta y} \tag{22}$$

Two questions must now be addressed. What upper limit L should be taken for j? What frequency values, $\tau$, should be calculated? For the first question assume that the N values of f(x) adequately sample that function. Then, since nonuniform sampling is used to evaluate Eq. (22), choose the largest increment in y to be less than or equal to $\Delta x$. This should ensure that f is adequately sampled in the "y" space. The largest increment occurs for maximum j so with

$$(N-1)\Delta x = \Delta x e^{(L-1)\Delta y} \tag{23}$$

the largest increment becomes

$$\Delta x = \Delta x e^{(L-1)\Delta y} - \Delta x e^{(L-2)\Delta y} \tag{24}$$

Combining these equations

$$L = 1 + \ln(N-1)/\ln((N-1)/(N-2)) \tag{25}$$

$$\Delta y = \ln((N-1)/N-2)) \tag{26}$$

For later convenience choose L instead to be

$$L=2^n \tag{27}$$

where n is chosen sufficiently large to satisfy Eq. (25). Equation (26) then becomes

$$\Delta y = \frac{1}{2^n-1} \ln(N-1) \tag{28}$$

The second question can be answered by rewriting Eq. (22) in the form of a discrete Fourier transform. To do this the argument of the phase factor must be altered to

$$j\tau\Delta y = 2\pi jk/L \tag{29}$$

Thus

$$\tau = 2\pi k/L\Delta y \qquad |k| \leq L-1 \tag{30}$$

are the desired frequencies with increment

$$\Delta\tau = 2\pi/L\Delta y \tag{31}$$

The Mellin transform from Eq. (22) can now be written as the discrete Fourier transform

$$M(k) \simeq (\Delta x)^{\sigma+ik\Delta\tau}\Delta y \sum_{j=-(L-1)}^{L-1} f(\Delta x e^{j\Delta y}) e^{j\sigma\Delta y} e^{i2\pi jk/L} \tag{32}$$

When j is zero in Eq. (21), x becomes $\Delta x$. The sum in Eq. (32) can then be broken into two parts corresponding to $j<0$ and $j\geq 0$. The second part requires sampling f(x) for $\Delta x \leq x \leq (N-1)\Delta x$. Since equal increments in y do not correspond to values $j\Delta x$, f(x) must be interpolated. The interpolation can be performed by fitting a parabola to three successive values of $f(j\Delta x)$. The desired value f(x) is found by evaluating the parabola at x. A sequence of numbers is thus formed which can be Fourier transformed using the Fast Fourier Transform (FFT) algorithm with its associated computational advantage.

The first part of the sum in Eq. (32) may be evaluated in a similar manner. Here, however, the interpolation is performed for $0 \leq x \leq \Delta x$. The only data values available are f(0) and $f(\Delta x)$. The final desired transform is the Fourier-Mellin transform. This uses the magnitude of the Fourier transform as the input to a Mellin transform. The magnitude of the Fourier transform is real and symmetric about zero, however. Therefore, again use a parabola as the interpolating function but force it to be symmetric about zero. To do this use the three successive values $(-\Delta x, f(\Delta x))$, $(0, f(0))$, $(\Delta x, f(\Delta x))$. By using a single interpolating

function over the entire range, the sum over negative j in Eq. (32) may be computed analytically and merely evaluated at the appropriate frequencies $\tau$. The Mellin transform in Eq. (32) is then the sum of the two parts described above.

An alternative method of approximating the Mellin transform is given in Ref. {5}. They also divide Eq. (32) into two parts and treat the second part essentially the same as described above. To evaluate the first part they assume that f(x) can be approximated by a constant

$$f(x) \approx f(0) \qquad 0 \leq x \leq \Delta x \tag{33}$$

Then from the definition

$$M_1(s) \approx f(0) \int_0^{\Delta x} x^{s-1} dx = f(0) \left(\frac{\Delta x}{s}\right)^s \tag{34}$$

where $M_1$ is the contribution from the sum over negative j.

Casasent and Psaltis[6, 7] discuss the space bandwidth requirements to implement the Mellin transform. They consider an input function defined over $0 \leq x \leq x_{max}$. Using Eq. (13) this is equivalent to $-\infty < y \leq \ln(x_{max})$. Instead let $x_{min} \leq x \leq x_{max}$ to avoid the problems introduced near $y=-\infty$. Also, assume that $x_{min}=k\Delta x$ and $x_{max}=N\Delta x$ where $\Delta x$ is the sampling increment in x space. In other words, the first k samples of the input function are excluded.

To find the resolution or sample increment in y space

$$\Delta y = \frac{d(\ln x)}{dx} \Delta x = \frac{\Delta x}{x} \tag{35}$$

The worst case in terms of the required number of samples in y space is

$$\Delta y = \frac{\Delta x}{x_{max}} = \frac{\Delta x}{N\Delta x} = \frac{1}{N} \tag{36}$$

The required number of y samples (space bandwidth) is then given by

$$L=(y_{max}-y_{min})/\Delta y$$

$$=N\left[\ln(N\Delta x)-\ln(k\Delta x)\right] = N\ln(N/k) \qquad (37)$$

Recall that the Mellin transform is to be used with scaled functions f(ax) where a is the scale factor. The number of samples k that are effectively excluded is proportional to a. Letting $k_1$ be the number of excluded samples when a=1,

$$k=ak_1 \qquad (38)$$

The required space bandwidth is then

$$L=N\ln(N/k_1)=N\ln(aN/k) \qquad (39)$$

with k/N considered to be proportional to the accuracy.

Table 1 lists a few space bandwidths L calculated from Eq. (39). Also shown are the number of sample points calculated using Eqs. (25) and (27). The values from Eqs. (25) and (27) are much larger than those from Eq. (39) for the cases shown. Using L=4096 and an accuracy k/N=0.01, scale factors of nearly 30 should be possible. Equivalently with a scale of a=3 the accuracy may be k/N=0.001.

TABLE 1

SPACE BANDWIDTHS REQUIRED TO EVALUATE THE MELLIN TRANSFORM

| N | k/N Accuracy | a Scale | L (39) | L (25) | L (27) |
|---|---|---|---|---|---|
| 512 | 1% | 2 | 2713 | 3185 | 4096 |
| 512 | 1% | 3 | 2920 | 3185 | 4096 |
| 512 | 2% | 2 | 2358 | 3185 | 4096 |
| 512 | 2% | 3 | 2566 | 3185 | 4096 |

## 4. TRANSFORMS OF TEST FUNCTIONS

This section presents examples of Mellin and Fourier-Mellin transforms of simple test functions. Rectangle and gaussian functions are chosen to provide better physical understanding of the transform operation. The test functions are easy to visualize but yet can be considered as fundamental components of more complicated functions. The real part of s, $\sigma$, is chosen equal to 1 for all examples.

First consider the Mellin transform of a rectangle function. Using 128 sample points, the magnitudes of Mellin transforms are shown in Fig. 2. Two rectangles are transformed separately, one of width 20 sample points and the other of width 60.

$$f(x) = \begin{cases} 8 & 0 \le x < w\Delta x \\ 0 & w\Delta x \le x \le x_{max} \end{cases} \qquad w=20,60 \tag{40}$$

Figure 2 includes both analytic and digitally implemented transforms for both rectangle sizes. The analytic transform is performed over the range $x_{min} \le x \le x_{max}$ to correspond to the digital implementation, Eq. (32), and to avoid the difficulties near x=0.

$$M(\nu) = \int_{x_{min}}^{x_{max}} f(x) x^{i2\pi\nu} dx \tag{41}$$

Using Eqs. (25) and (27), L=1024,

$$x_{min} = \Delta x \exp(-(L-1)\Delta y) \tag{42}$$

and

$$M(\nu) = \left[ (w\Delta x)^{1+i2\pi\nu} - (x_{min})^{1+i2\pi\nu} \right] / (1+i2\pi\nu) \tag{43}$$

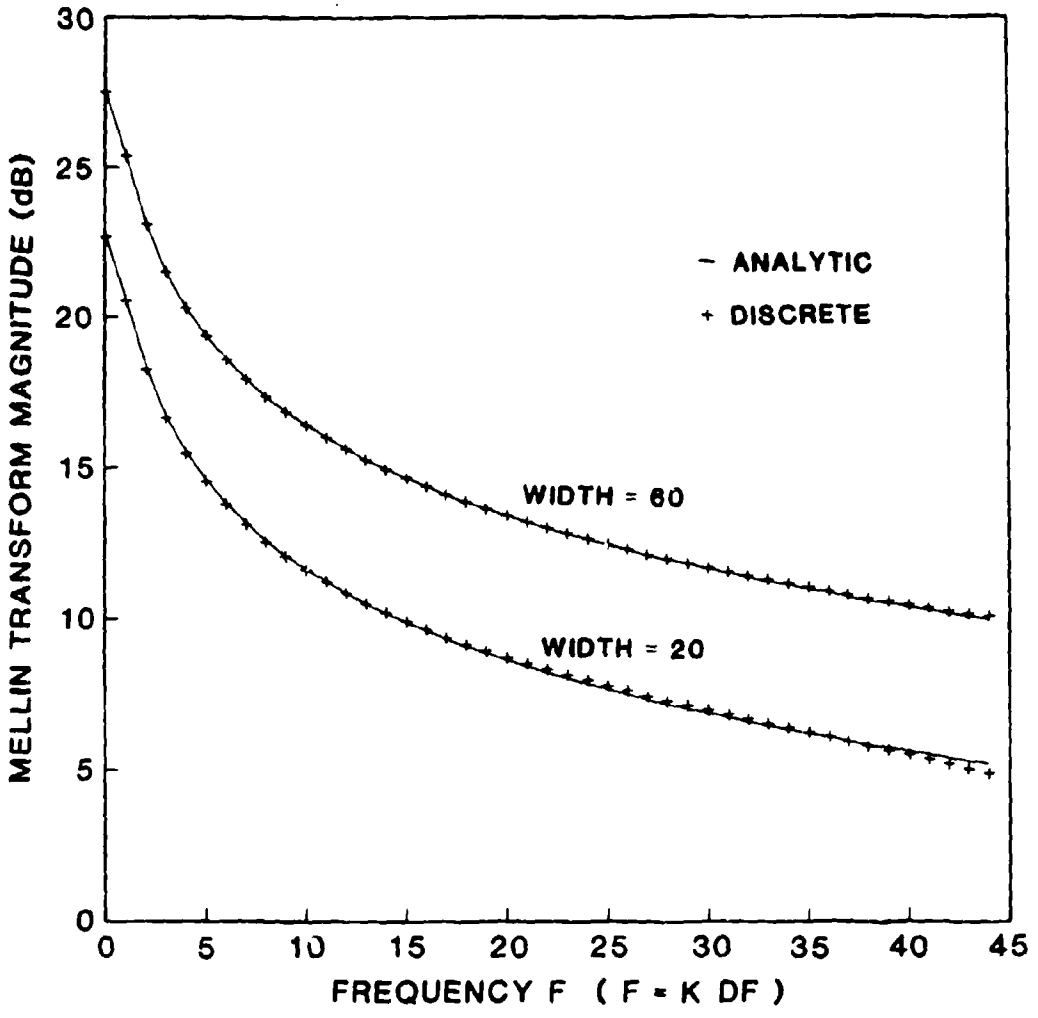


Fig. 2. Magnitudes of Mellen transforms of rectangle test functions, one three times wider than the other. Note the close agreement between the analytic and discrete transforms. The rectangle widths are evident in the factor of 3 or 4.77 dB difference in transform magnitudes.

Figure 2 shows the close agreement between the two transform methods. Also shown is the effect of the factor of three scaling between the two test functions, evident here as a constant additive factor due to the logarithmic scale. This is consistent with Eq. (6) where a=1/3 and c=1 and illustrates the scale invariance of the Mellin transform.

There are small deviations between the analytic and digital results. This is to be expected since the discrete implementation in Eq. (32) is an approximation. Indeed, the approximation is equivalent to the rectangle rule for numerically evaluating an integral. There are higher order methods available for approximating integrals, but Eq. (32) is convenient and relatively efficient since the FFT algorithm is applicable.

Figure 3 shows Fourier and Mellin transforms of rectangle functions. Magnitudes of the transforms are plotted on linear scales. In Fig. 3a the left edge of the rectangle is located at the origin. Figure 3b shows the rectangle shifted to the right but with the same width. The magnitude of the Fourier transform, being shift invariant, is identical to that in Fig. 3a in agreement with Eq. (5). The magnitude of the Mellin transform is clearly different for the two cases illustrating that the Mellin transform is not shift invariant. Figure 3c shows transforms of a rectangle three times as wide. The transform magnitudes are all divided by three. The Mellin transform is now identical to that in Fig. 3a again illustrating scale invariance. The Fourier transform is compressed in frequency by a factor of three consistent with Eq. (9) and is not scale invariant.

Next consider transforms of gaussian shaped test functions. This is again a case where the Mellin transform can be performed analytically.

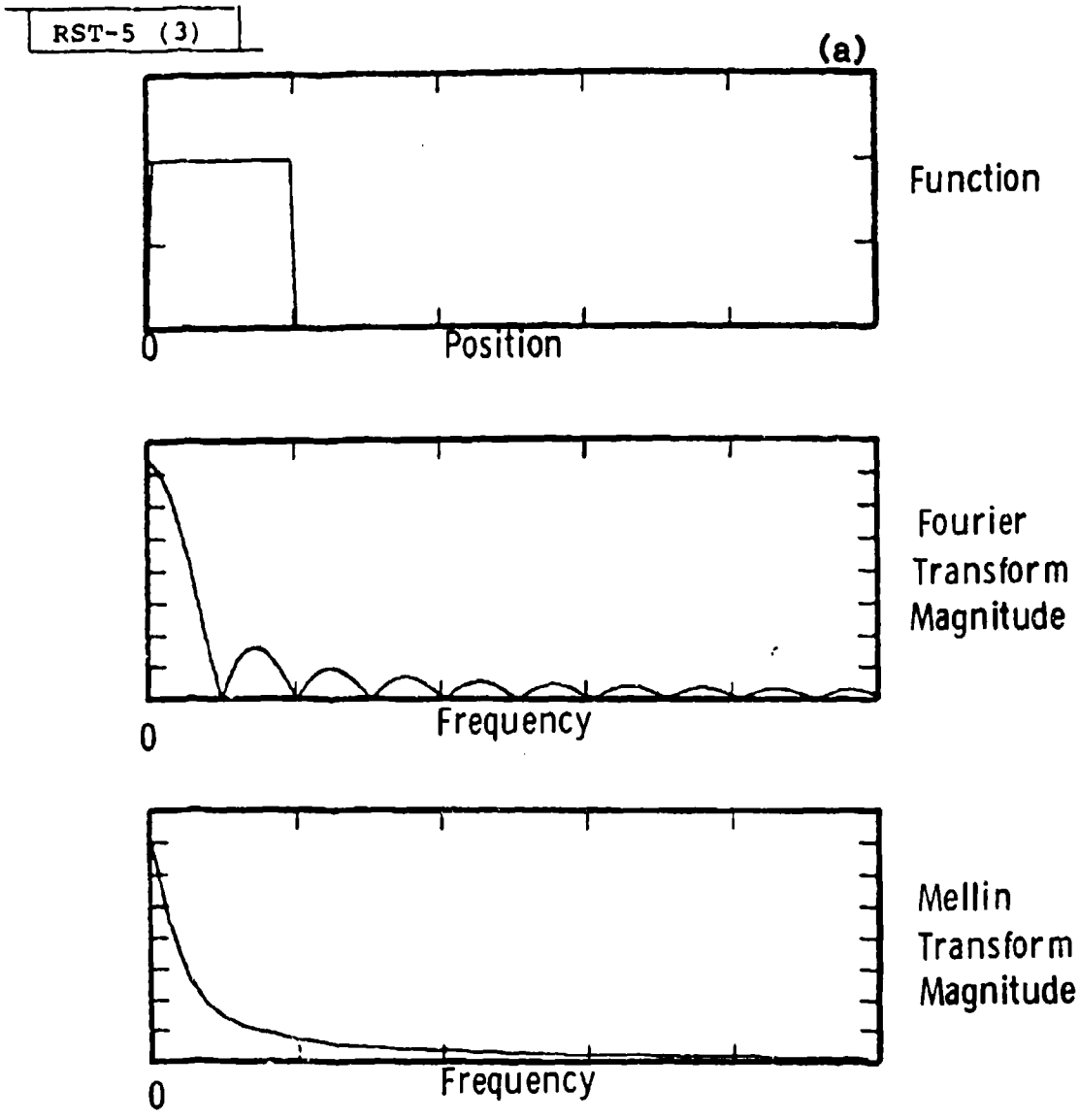


Fig. 3. Fourier and Mellin transforms of a rectangle test function illustrating how the magnitude of the Fourier transform is shift invariant while the magnitude of the Mellin transform is not. Similarly the Mellin transform magnitude is scale invariant while the Fourier transform magnitude is not.

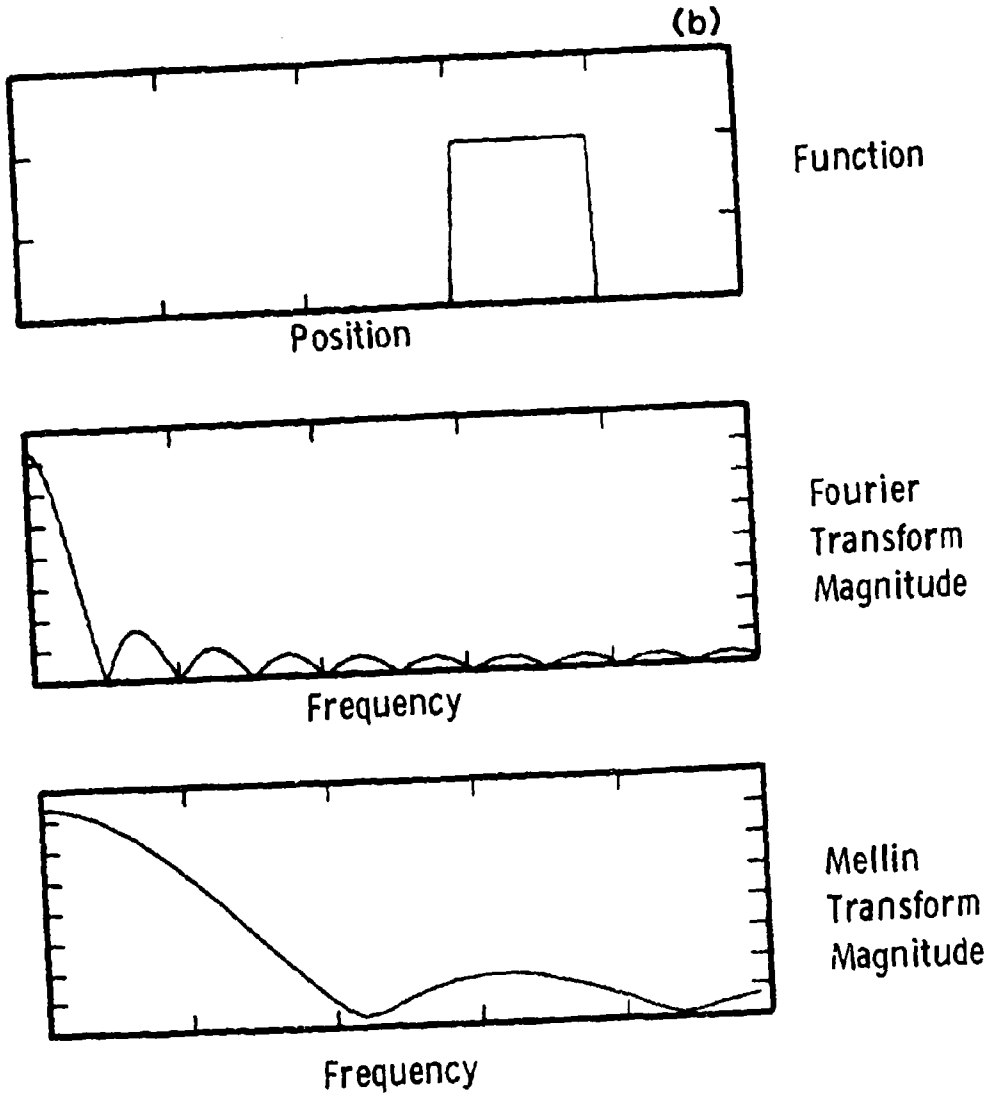
(b)
Function
Position
Fourier
Transform
Magnitude
Frequency
Mellin
Transform
Magnitude
Frequency

Fig. 3 (CONT'D)

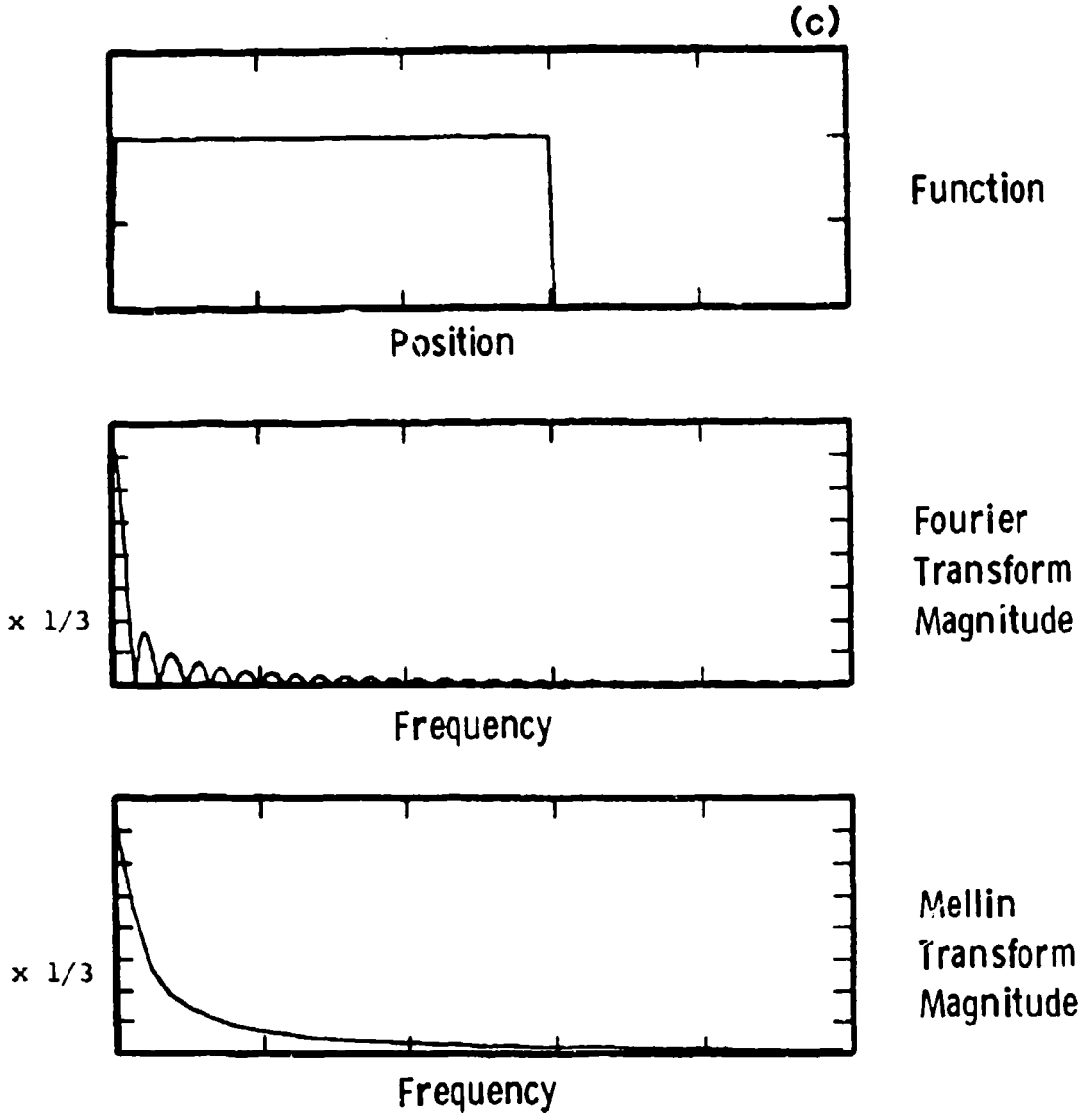
(c)
Function
Position
x 1/3
Fourier
Transform
Magnitude
Frequency
x 1/3
Mellin
Transform
Magnitude
Frequency

Fig. 3 (CONT'D)

$$M(s) = \int_0^\infty e^{-x^2} x^{s-1} dx = \tfrac{1}{2}\Gamma(\tfrac{1}{2}s) \quad \text{Re } s>o \tag{44}$$

With $s=1+i2\pi\nu$

$$M(\nu) = \tfrac{1}{2}\Gamma(\tfrac{1}{2}+i\pi\nu) \tag{45}$$

$$|M(\nu)| = \tfrac{1}{2}\left[\pi/\cosh\pi^2\nu\right]^{\frac{1}{2}} \tag{46}$$

Figure 4 shows the results of analytic and discrete Fourier-Mellin transforms of two gaussian test functions, one four times wider than the other. Analytic results are independent of width consistent with the Mellin scale invariance. The hyperbolic cosine in Eq. (46) causes the transform magnitudes to fall exponentially with frequency.

The constant increment used to sample the test functions causes the difference between the analytic and discrete calculations. In the discrete case the functions are approximated as series of rectangles. The Mellin transform is then a complex superposition of Mellin transforms of these rectangles. The larger number of finite samples from the wider test function is equivalent to using a smaller increment for the narrower function and leads to more accurate results.

Gaussian functions are also used in Fig. 5. Here the location and width of the gaussian are varied. The magnitudes of the Fourier and Fourier-Mellin transforms are shown along with the gaussian function. The Fourier transform is invariant to shift but not to scaling of the function width. Figures 5a and 5b illustrate this behavior as well as the combined shift and scale invariance of the Fourier-Mellin transform. The Fourier-Mellin transform is the same as the width=4 transform in Fig. 4. The kink in the transform near -40 dB is caused by not allowing the magnitude to be less than -40 dB for plotting. Figure 5b is scaled by 2 relative to Fig. 5a.

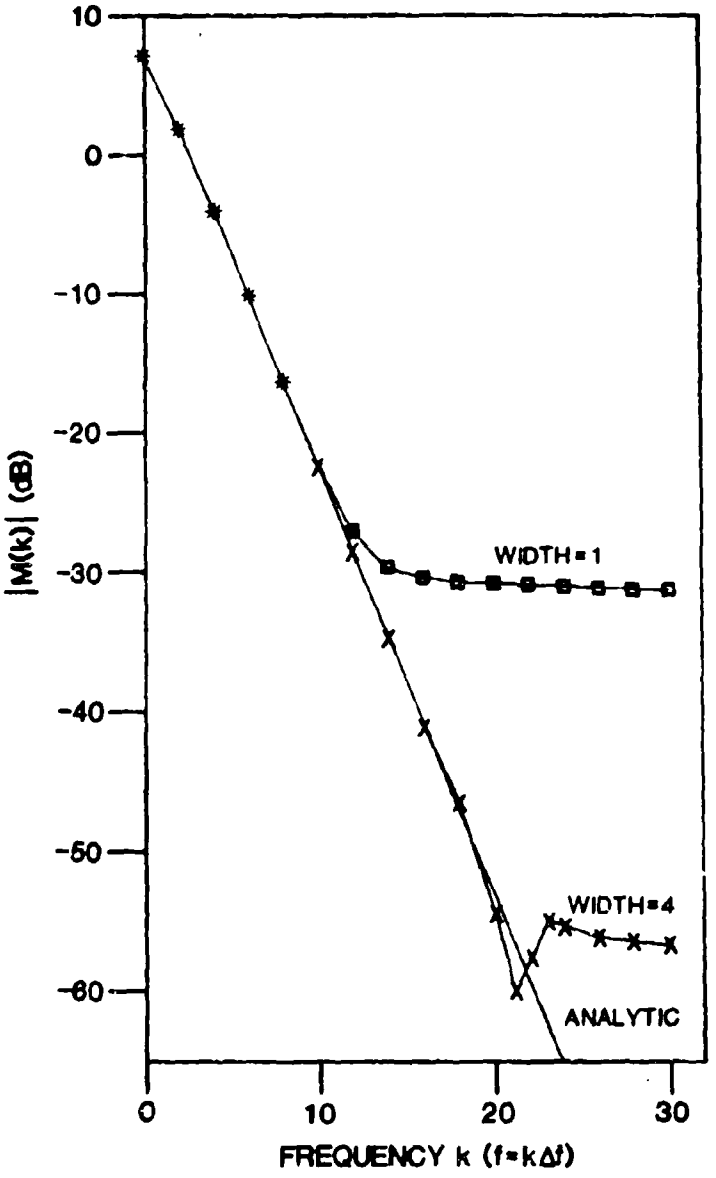


Fig. 4. Fourier-Mellin transforms of qaussian test functions. The two discrete transforms use the same sample increment and number of samples, but one test function is 4 times wider than the other. An analytic transform which is independent of the function width is shown for comparison.

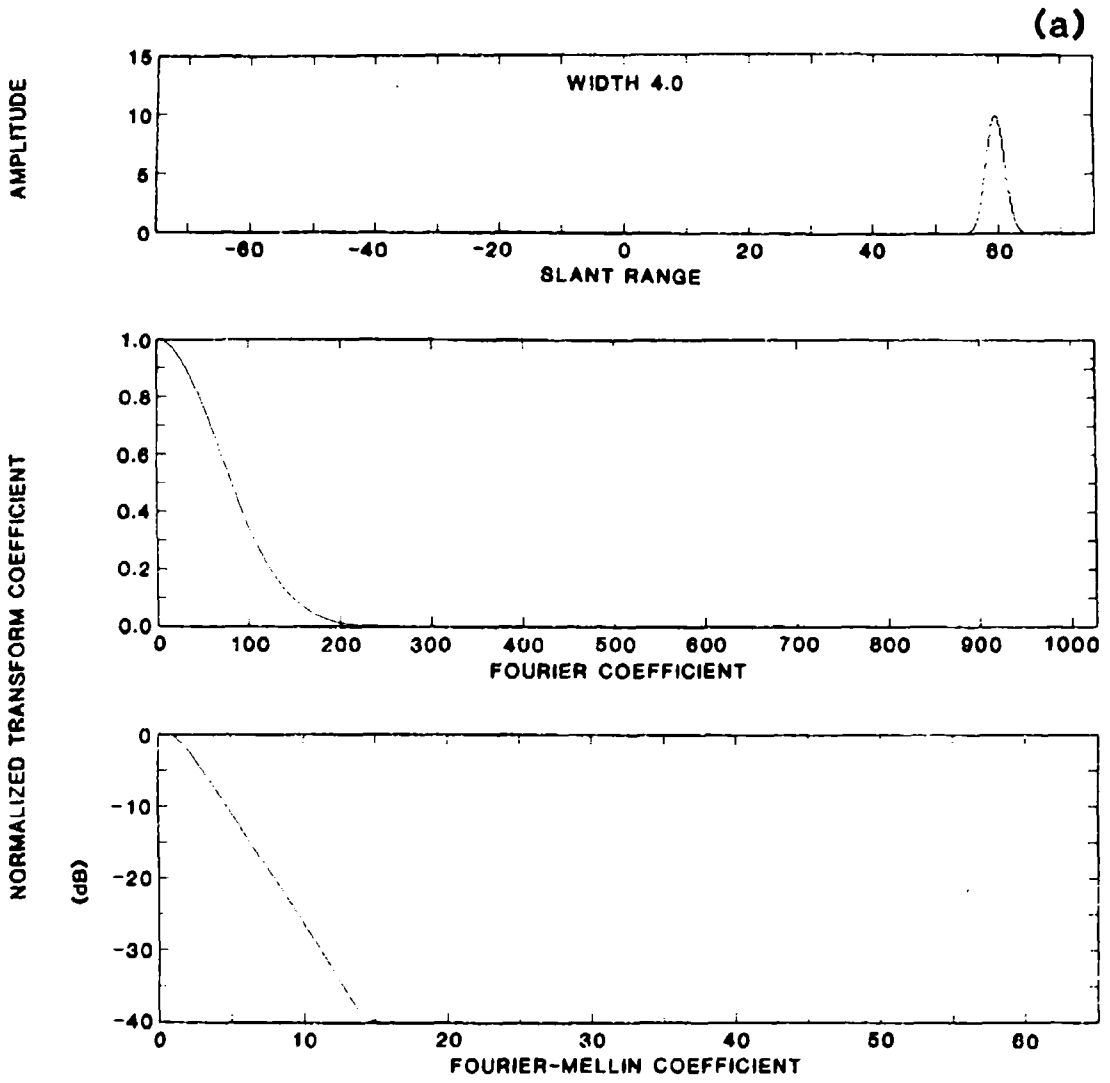


Fig. 5. Fourier and Fourier-Mellin transforms of sampled gaussian test functions illustrating the effects of shift and scale operations. Note also the effects produced by undersampling of the test function.

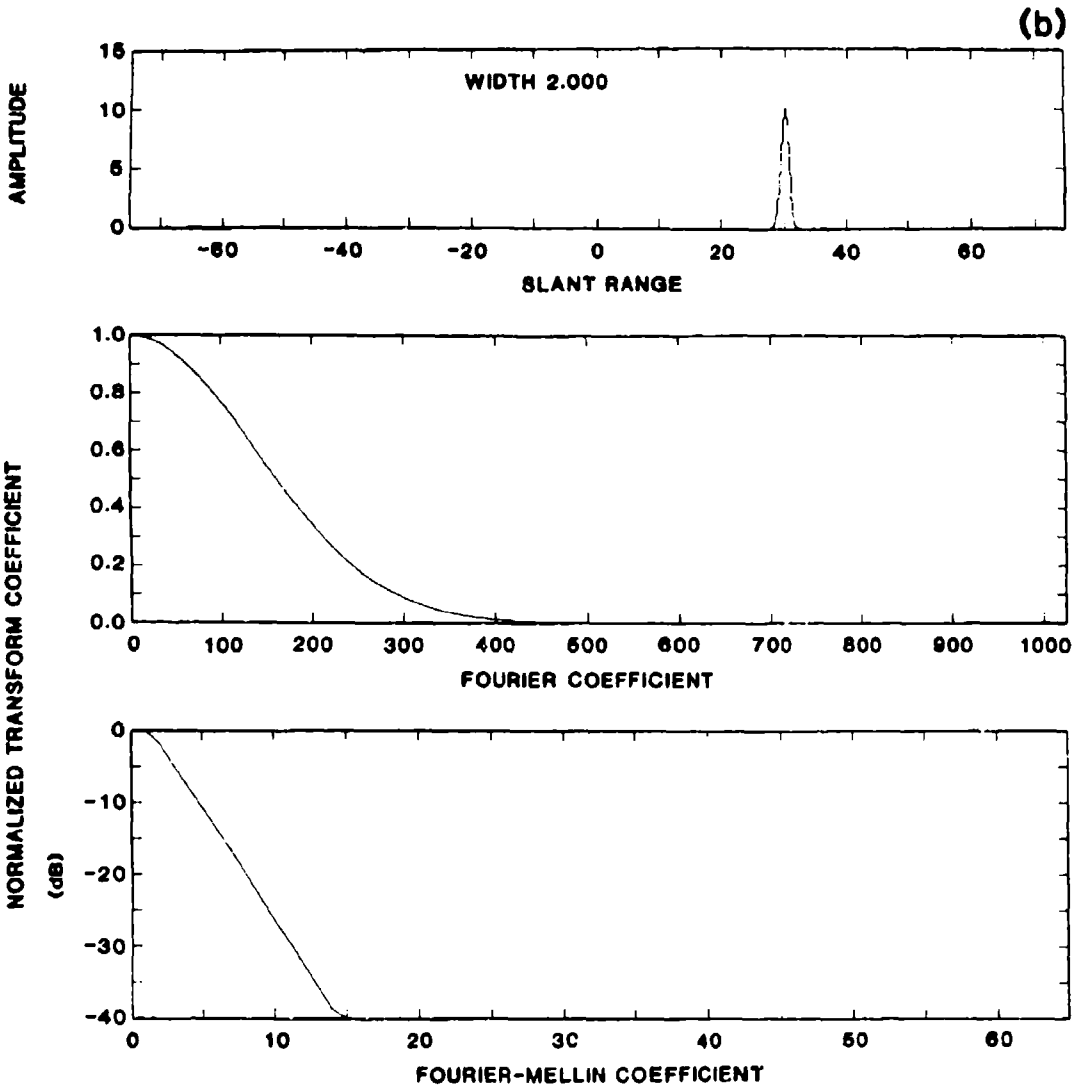
(b)
WIDTH 2.000
AMPLITUDE
15
10
5
0
-60
-40
-20
0
20
40
60
SLANT RANGE
NORMALIZED TRANSFORM COEFFICIENT
1.0
0.8
0.6
0.4
0.2
0.0
0
100
200
300
400
500
600
700
800
900
1000
FOURIER COEFFICIENT
(dB)
0
-10
-20
-30
-40
0
10
20
30
40
50
60
FOURIER-MELLIN COEFFICIENT

Fig. 5 (CONT'D)

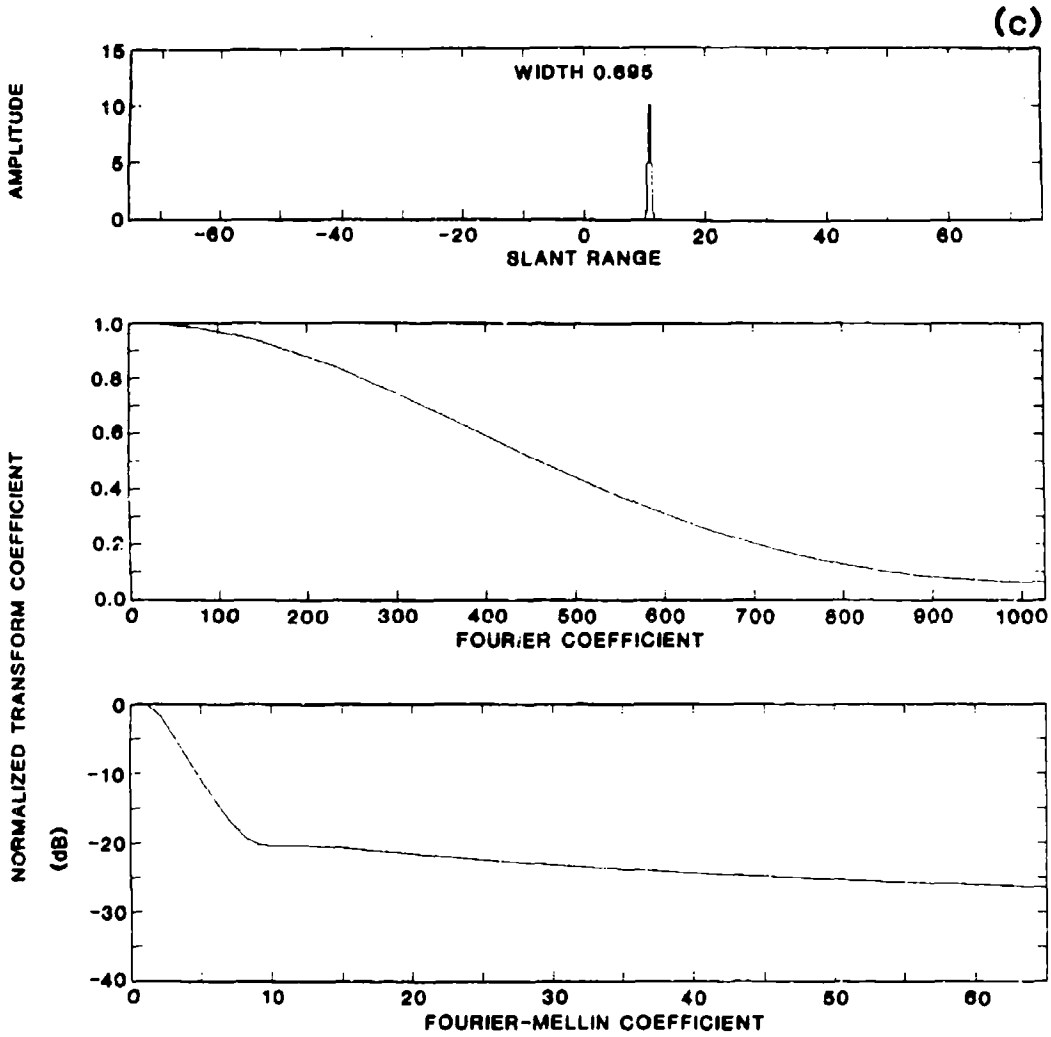
(c)
WIDTH 0.695
AMPLITUDE
15
10
5
0
-60
-40
-20
0
20
40
60
SLANT RANGE
NORMALIZED TRANSFORM COEFFICIENT
1.0
0.8
0.6
0.4
0.2
0.0
0
100
200
300
400
500
600
700
800
900
1000
FOURIER COEFFICIENT
(dB)
0
-10
-20
-30
-40
0
10
20
30
40
50
60
FOURIER-MELLIN COEFFICIENT

Fig. 5 (CONT'D)

Figure 5c is scaled by a factor of 5.76. This makes the test function narrower than the width=1 in Fig. 4. As expected the effectively lower sampling rate results in less accurate transform values. Also notice that in this case the frequency bandwidth of the input function exceeds the folding frequency of the Fourier transform. The Mellin transform is performed on the Fourier spectrum as shown. Since this spectrum is not a scaled version of the two previous spectra due to the finite value at the highest frequency, the Mellin transform values should not be identical.

The last series of calculations was also used to check Parseval's theorem between a function and its transform, Eqs. (17) and (18). The results are summarized in Table 2. Equation (17) for the Fourier transform holds for all cases. The approximation inherent in Eq. (32) is again evident for the Mellin transform in Eq. (18). An analytic calculation shows that both sides of Eq. (18) should equal 7.9577. The discrepancy between this value and those found using the discrete transform led to interpolating the Fourier frequency spectrum. This is done by appending zeros to the input function and performing a lengthened transform. The interpolation decreases the size of the frequency increment while increasing the number of increments. This should increase the accuracy attained in evaluating the Mellin transform using Eq. (32). Increasing the number of samples taken from the input function would be better, but is not always possible due to hardware constraints.

The energy of the weighted Fourier transform, the left-hand side (LHS) of Eq. (18), may be made to closely approach the analytic value. Summing the energy of the Mellin transform only over the first 65 coefficients led to consistently higher values for the right-hand side (RHS) of Eq. (18). Since only a portion of the total number of Mellin coefficients was summed, the

TABLE 2

PARSEVAL'S THEOREM FOR FOURIER AND MELLIN TRANSFORMS

| Scale Factor | Fourier Transform Eq. (17) | Mellin Transform Eq. (18) | | |
|---|---|---|---|---|
| | | LHS* | RHS* | RHS/LHS |
| 1.00 | 249.97 | 7.9531 | 8.0815 | 1.0161 |
| 1.31 | 191.49 | 7.9550 | 8.0816 | 1.0159 |
| 2.00 | 124.99 | 7.9566 | 8.0817 | 1.0157 |
| 5.76 | 43.50 | 8.0178 | 8.1389 | 1.0151 |
| Interpolate to ½ the sample increment | | | | |
| 1.00 | 249.97 | 7.9566 | 8.0198 | 1.0079 |
| 1.31 | 191.49 | 7.9571 | 8.0198 | 1.0079 |
| 2.00 | 124.99 | 7.9575 | 8.0198 | 1.0078 |
| 5.76 | 43.50 | 8.0174 | 8.0768 | 1.0074 |
| Interpolate to ¼ the sample increment | | | | |
| 1.00 | 249.97 | 7.9575 | 7.9888 | 1.0039 |
| 1.31 | 191.49 | 7.9576 | 7.9888 | 1.0039 |
| 2.00 | 124.99 | 7.9577 | 7.9888 | 1.0035 |

*LHS = Left-Hand Side

RHS = Right-Hand Side

resulting energy should be less than the LHS of Eq. (18). The difference is apparently due to the approximation in Eq. (32). This is unlike the Fourier case where Eq. (17) can be proven to hold exactly in the discrete case as well. The last column in Table 2 lists the ratio RHS/LHS for Eq. (18). This ratio is seen to approach one as the Fourier transform is smoothed by increasing the number of interpolating points. Increasing the number of Fourier frequency samples through interpolation improves the accuracy of the discrete Mellin transform of that Fourier spectrum.

The difficulties described above imply that the relative energy contributed by the first N Mellin coefficients can only be determined by first finding the energy of all the coefficients. This may be computationally expensive for pattern classification where only a few coefficients may be desired.

Finally in Fig. 6, results of ideal low pass filtering in the frequency domain are shown. The top panel shows the input function. The middle and lower panels show the results of filtering in the Fourier and Mellin frequency domains, respectively. For both cases a forward transform is performed. Filtering is done by retaining the first N complex coefficients and zeroing all higher ones. Finally an inverse transform is performed to return to the space domain. Note that the phase information associated with those N coefficients in the frequency domain is not discarded as it is in performing the Fourier-Mellin transform. The ringing near the origin in the Mellin results arises in the inverse Mellin transform and does not affect the results presented next.

As expected increasing the number of coefficients retained by the filter increases the fidelity of the resulting space functions. The fidelity for the Fourier case is independent of the position of the rectangle pulse. This is not true for the Mellin case. Here the fidelity is highest near the origin and becomes progressively worse for positions away from the origin.

RST-5 (6)

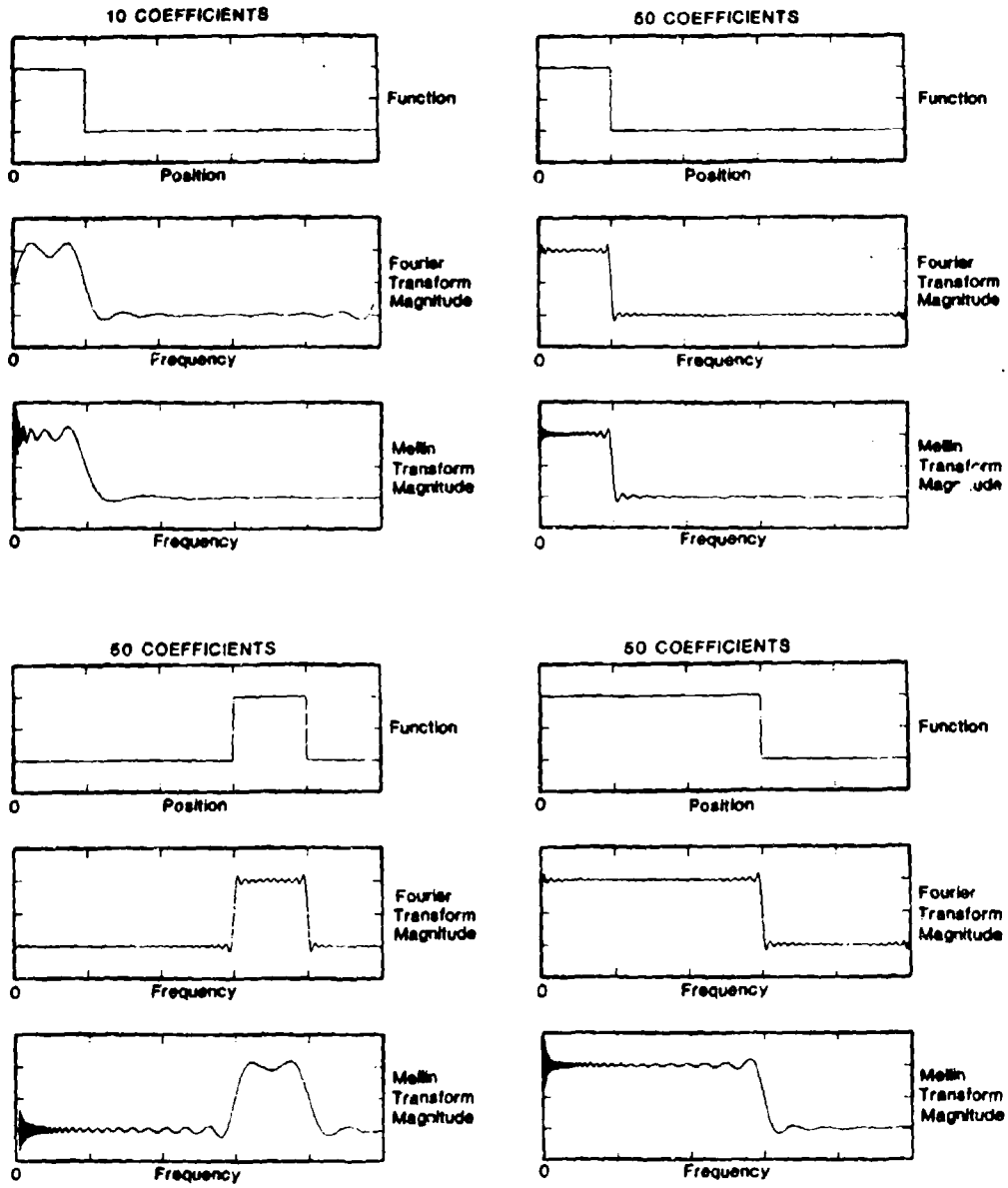


Fig. 6. Effects produced by rectangular low pass filters. The filters are applied in the Fourier and Mellin frequency domains. As expected, retaining higher frequency components results in better reproduction fidelity. The fidelity in the Mellin case depends on the function position.

These effects are due to fundamental differences in the two transforms (see Eqs. (3) and (12)). The Fourier transform may be thought of as a method to calculate the coefficients required to expand a function in a sinusoidal (i.e. Fourier) series. For a constant frequency the argument of the sinusoids increases linearly with x. Looking at the Mellin transform in the same manner, one finds that the argument of the corresponding sinusoids does not increase as x but rather as ln x. The fineness of detail that may be represented in both cases is roughly the oscillation period of the approximating functions. The constant period in the Fourier case means that a function may be approximated equally well regardless of the location of that function. This is not true in the Mellin case where a particular oscillation period near the origin can only be reproduced away from the origin by going to higher transform frequencies to compensate for the ln x term.

This section has considered applying Fourier, Mellin, and Fourier-Mellin transforms to relatively simple test functions. The exercise has provided insight into the physical operation of the transforms and their differences. The next section will consider transforms of more complicated functions more similar to those encountered in the real world.

## 5. TRANSFORMS OF SIMULATED SHIP PROFILES

In the previous section transforms of simple test functions were considered. Now more complicated functions will be used. These functions are computer generated, amplitude vs slant range, radar profiles of a simulated ship. The ship consists of 49 unit amplitude point scatterers located at representative three-dimensional positions. The radar is assumed to be viewing the ship at zero elevation angle but differing aspects. With this geometry the simulated radar profiles are independent of the height of the scatterers. Various aspects are found by effectively rotating the ship about a vertical axis through its center while keeping the radar position fixed. All distances are slant ranges along the RLOS and are measured relative to the rotation axis of the ship.

Several assumptions are made when using this model. No interference between scatterers occurs in the received waveform. There is no shadowing of scatterers by others, thus 49 point scatterers are always visible. Each scatterer is assumed to be represented by a guassian pulse in the received waveform. Corresponding to the unit amplitude of the scatterers, each gaussian has unit amplitude and all gaussians have identical width.

For a first example consider Fig. 7. Here the model has been further simplified by assuming that all scatterers lie along the centerline of the ship. The radar then views only a line of point scatterers. As the viewing aspect between the radar and the ship is altered, the scatterers remain in the same positions relative to each other but their absolute locations are scaled as the cosine of the aspect angle, $\alpha$. One additional assumption made is that the width of a point scatterer return is also scaled by cos $\alpha$. Then as the perceived length of the ship shortens, for example, the width of each scatterer return becomes narrower. This is done to make each profile a scaled version of the others.

The top panel of Fig. 7a shows the ship at zero aspect or along the length. The ship profile is merely the sum of the returns from all scatterers. The magnitude of the Fourier transform is plotted in the middle panel on a linear scale. The bottom panel shows the magnitude of the Fourier-Mellin transform with the vertical axis in dB.

Figure 7b shows the ship at a $60^{\circ}$ aspect. The scatterer width is 0.5 (cos $60^{\circ}$) that at $\alpha=0^{\circ}$. The profile is thus a scaled version of the one at $\alpha=0^{\circ}$. The Fourier transform is stretched relative to $\alpha=0^{\circ}$ but all of the structure remains. The Fourier-Mellin transform is nearly identical to the one at $\alpha=0^{\circ}$ for the portion shown. Only minor differences appear near the 60th coefficient. This Fourier-Mellin transform is nearly invariant to a scale change of a factor of two.

Figure 7c is at an $80^{\circ}$ aspect. Even at a scale factor of nearly six, the Fourier-Mellin transform begins to deviate from the one at $\alpha=0^{\circ}$ only near the 40th coefficient. Some deviation is expected since the individual gaussian widths are now on the same order as the sampling increment. The ship profile is more nearly a series of rectangular pulses than smooth gaussians.

In actual practice the radar return from a point target does not change as the aspect angle is varied, as is assumed in Fig. 7. Rather the return from a point target is constant in width regardless of the aspect angle due to the fixed range resolution of the radar. The locations of scatterers will scale with aspect but the scatterer widths will not. Since there is no longer pure scaling of the target, the Fourier-Mellin transform should not be invariant. This is seen in Fig. 8 where the same target is used as in Fig. 7, but the scatterer widths are not scaled. Comparing Fig. 8 at $\alpha=60^{\circ}$ with Fig. 7a at $\alpha=0^{\circ}$, the individual scatterers have coalesced producing a profile different from the one at $\alpha=0^{\circ}$. Comparing the Fourier-Mellin transforms, significant differences appear even in the second coefficient.

RST-5 (7)

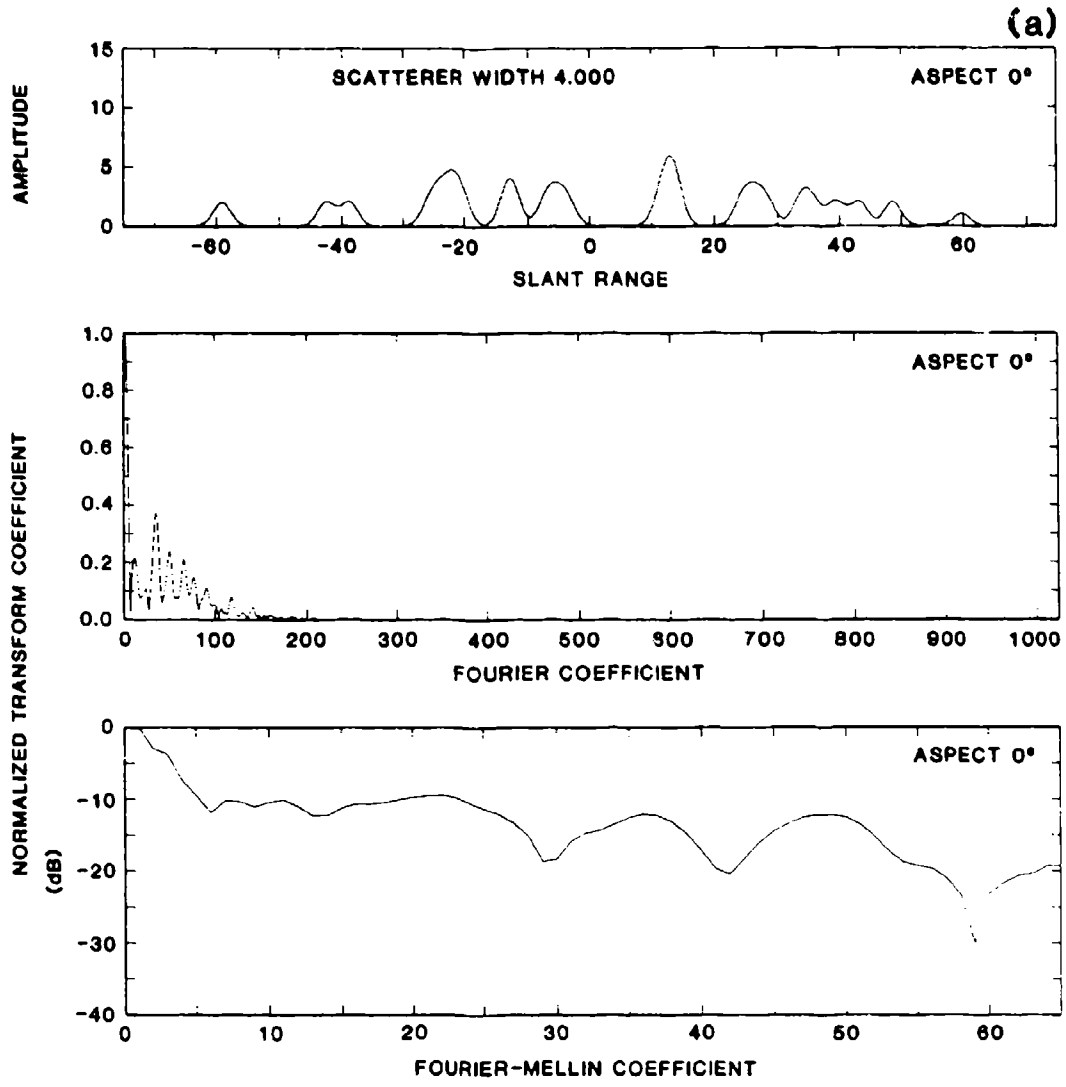


Fig. 7. Fourier and Fourier-Mellin transforms of simulated ship profiles are shown at three aspect angles, $\alpha$. The simulated ship consists of 49 colinear point scatterers along the centerline of the ship. The simulated radar range resolution is scaled by $\cos\alpha$. The profiles are scaled versions of each other and show the near scale invariance of the Fourier-Mellin transform.

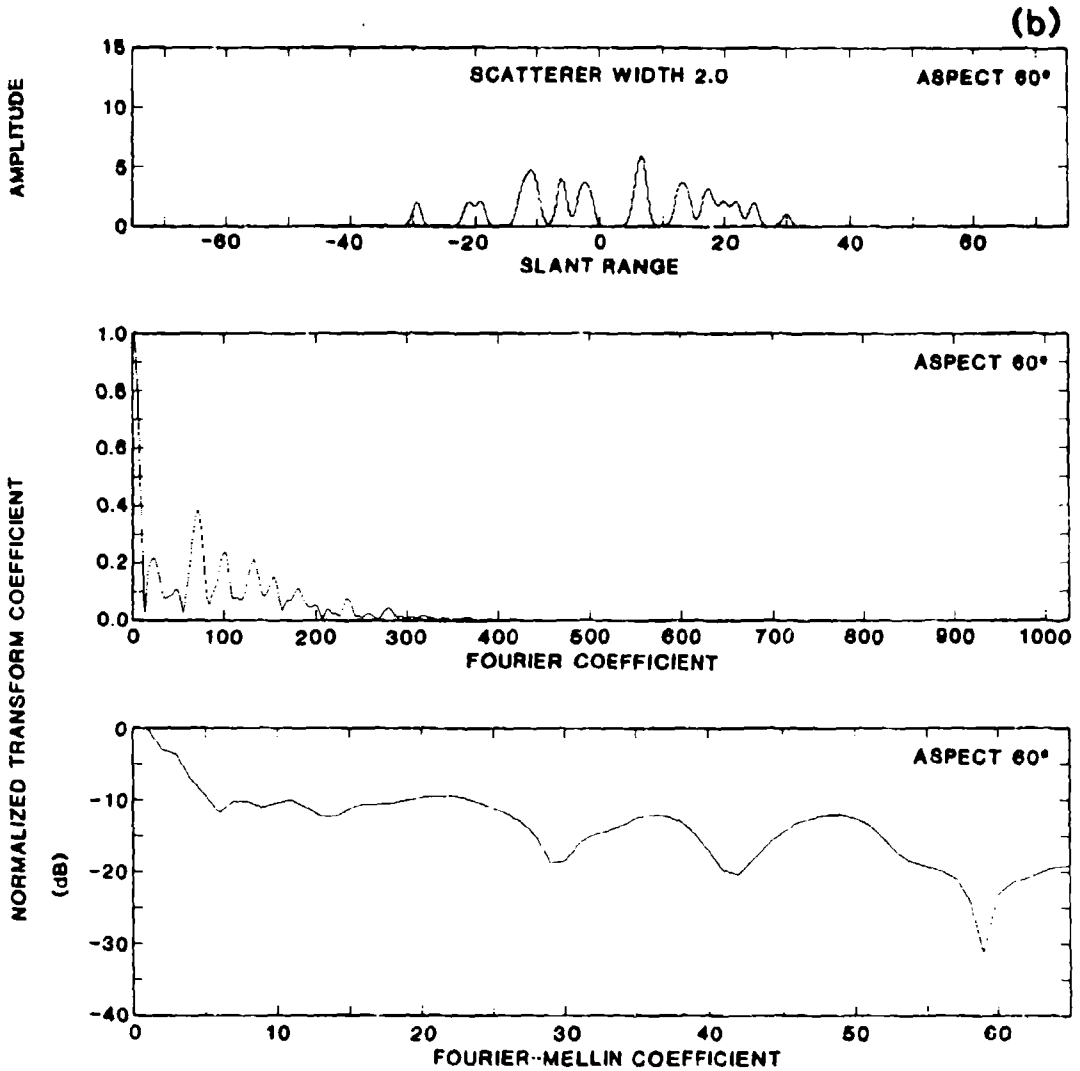
(b)
SCATTERER WIDTH 2.0
ASPECT 60°
AMPLITUDE
15
10
5
0
-60
-40
-20
0
20
40
60
SLANT RANGE
ASPECT 60°
NORMALIZED TRANSFORM COEFFICIENT
1.0
0.8
0.6
0.4
0.2
0.0
0
100
200
300
400
500
600
700
800
900
1000
FOURIER COEFFICIENT
ASPECT 60°
(dB)
0
-10
-20
-30
-40
0
10
20
30
40
50
60
FOURIER-MELLIN COEFFICIENT

Fig. 7 (CONT'D)

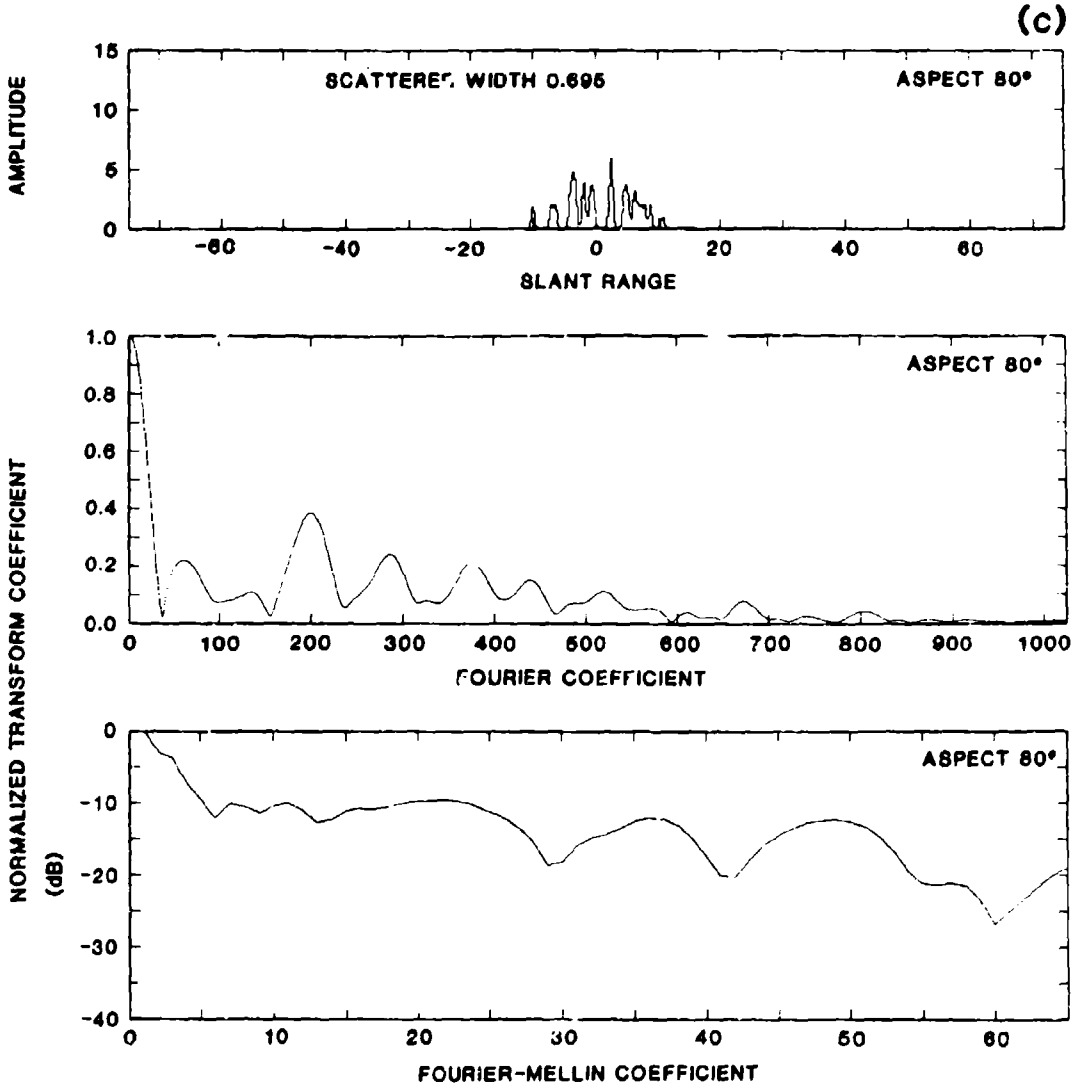
(c)
SCATTERER WIDTH 0.695
ASPECT 80°
AMPLITUDE
SLANT RANGE
ASPECT 80°
NORMALIZED TRANSFORM COEFFICIENT
FOURIER COEFFICIENT
ASPECT 80°
(dB)
FOURIER-MELLIN COEFFICIENT

Fig. 7 (CONT'D)

RST-5 (8)

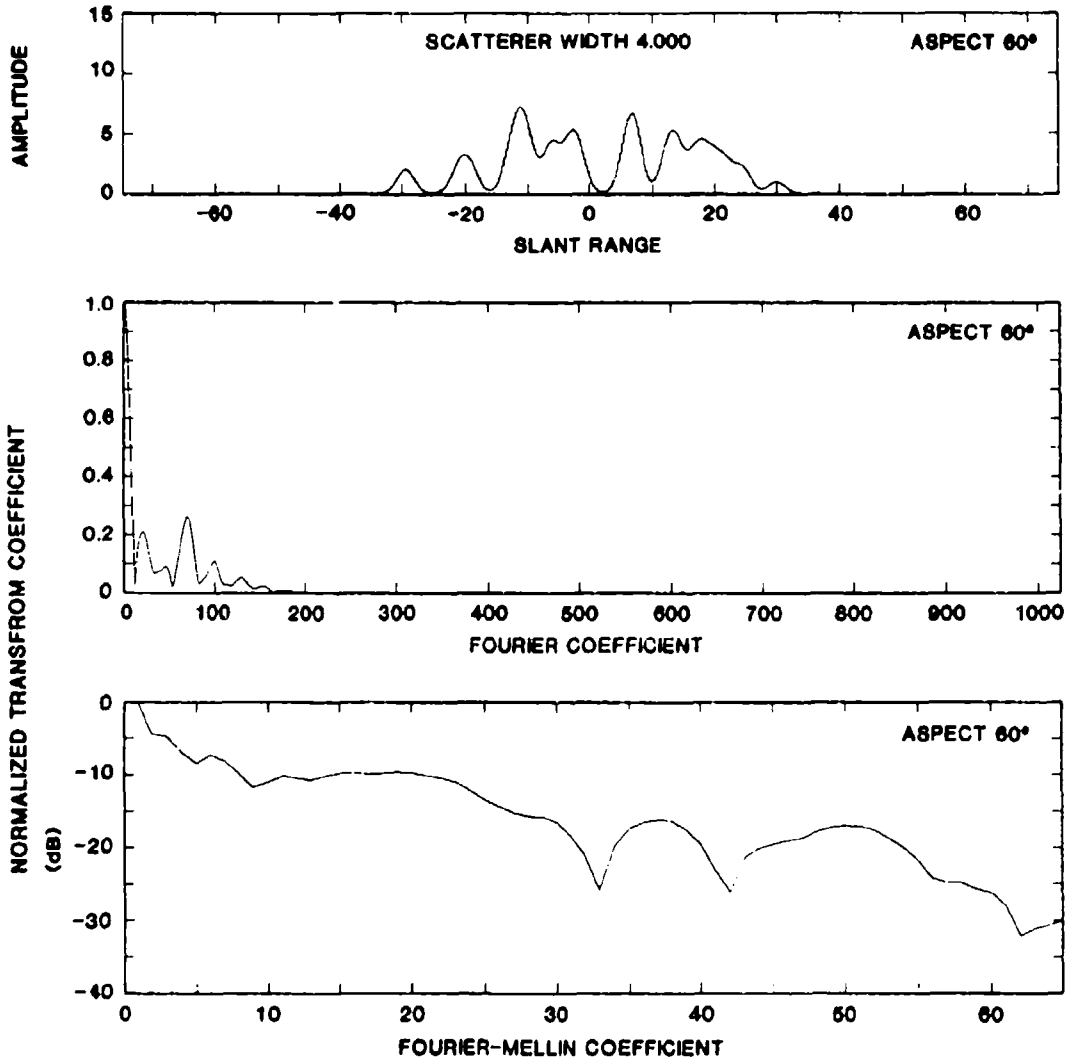


Fig. 8. Effects of constant radar range resolution are shown for an aspect of 60°.

Conditions actually encountered are generally worse than those considered so far. Targets are rarely arrays of colinear point scatterers. Instead the scatterers are distributed in three dimensions, there is interference between scatterers, and it is possible to shadow scatterers by others. Figure 9 shows the same ship profile as before at $\alpha=60^{o}$ but with the scatterers in three dimensions. There is still no interference or shadowing allowed. Clearly this profile is not a scaled version of the profile in Fig. 7a. It is not easy to identify this profile as being from the same ship. As expected the Fourier-Mellin transforms differ substantially even in the first coefficients.

For more complicated profiles such as those considered here, the Fourier-Mellin transform as implemented is scale invariant to a good approximation so long as the profiles are actually scaled. When effects typical of more realistic profiles are included, scaling does not apply and the Fourier-Mellin transforms of these profiles are not scale invariant.

RST-5 (9)

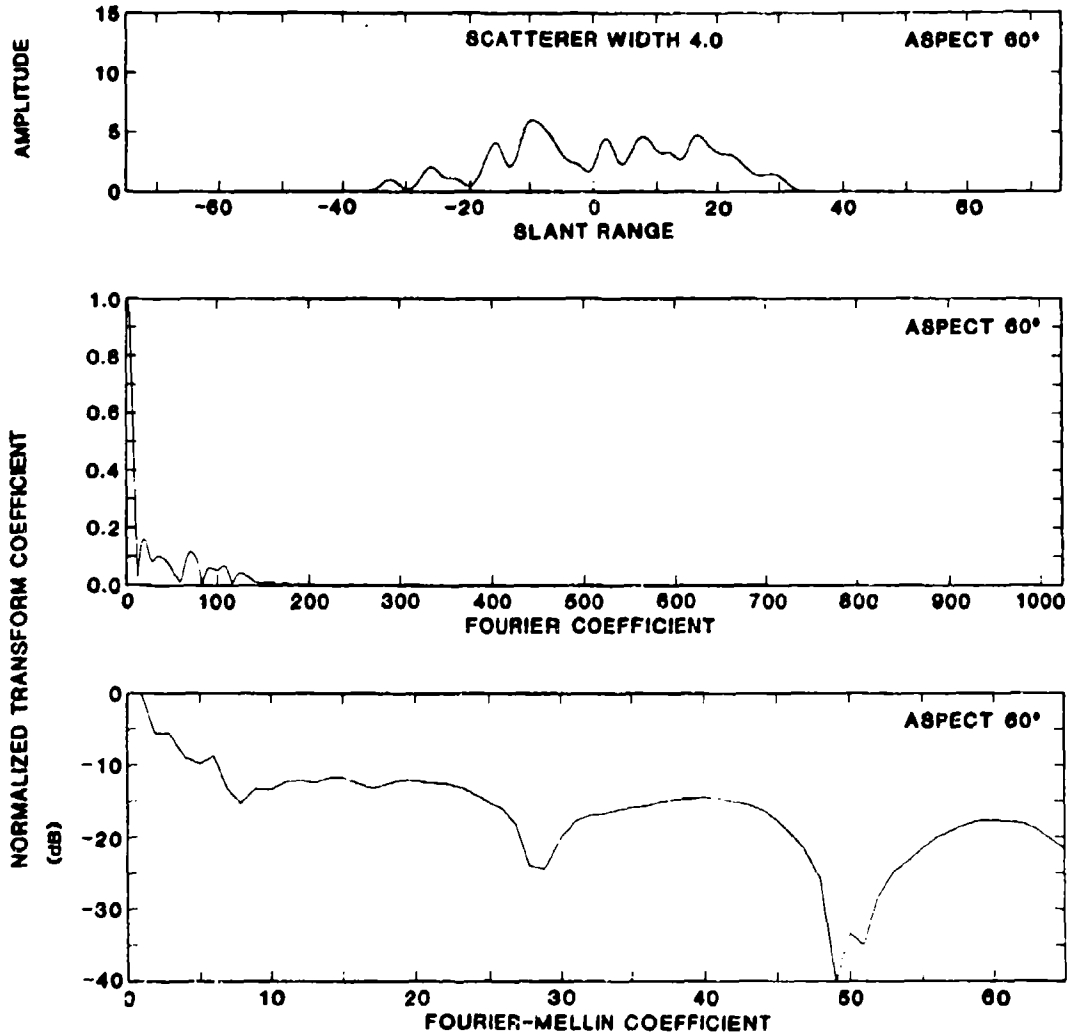


Fig. 9. The effects of using constant radar range resolution and a three-dimensional distribution of point scatterers are shown for an aspect of 60°. The profile and its transforms differ significantly from those in Figs. 7b and 8. This emphasizes that aspect is not equivalent to scale for these conditions.

## 6. AUTOMATIC SHIP CLASSIFICATION

It was indicated in the previous section that realistic radar ship profiles do not merely scale by the cosine of the aspect angle. Both the Fourier and the Fourier-Mellin transforms therefore depend on aspect. The question is then whether the Fourier-Mellin transform is able to achieve at least partial aspect independence and result in ship classification performance better than that achieved using the Fourier transform. Using the magnitude of the Fourier-Mellin transform for feature selection, simple linear and quandratic classifiers are used on both simulated and real ship profiles. For comparison the same classification techniques are repeated using the magnitude of the Fourier transform as the feature selector. Better classification in terms of lower equal error rates* is the criterion used in the comparison.

Profiles for each degree of aspect ($0^{o}$ to $180^{o}$) are generated for two ships using the simulated model. The two groups of profiles are then each divided into a training and a testing set using alternate profiles. The training sets are used to train the linear and quadratic classifiers. The classifiers are tested using both the training and testing sets independently. Classification results obtained from the training sets should be optimistic. Results obtained from the testing sets are also probably biased since the training and testing sets are constructed

---

*The measure of performance is the equal classification error probability as derived from the operating characteristic curve. This O-C curve is a plot of the probability of incorrectly classifying class 1 vs the probability of incorrectly classifying class 2 and is obtained by calculating these probabilities as a function of a threshold and then varying the threshold. The point where these probabilities are equal is called the equal classification error probability and is often used as a simplified measure of the operating characteristic.

using alternate profiles which are unlikely to be totally independent. The conditions for the comparison between the Fourier-Mellin and the Fourier transforms are identical, however, so the relative performance of each transform should be valid.

Figures 10 and 11 show the classification results for the two transforms as a function of the number of transform coefficients used. The linear classifier results in Fig. 10 are very comparable. Neither technique is consistently better than the other. The quadratic classifier results in Fig. 11 are similar. Again neither technique outperforms the other. The overall classification performance on the simulated ship profiles is better using the quadratic rather than the linear classifier.

Next the same techniques are applied to actual radar ship profiles. Data from two ships, an FF, and a DD, are used. Profiles from each ship are available at approximately one degree aspect increments. One training and two testing sets are formed for each ship by assigning every third profile to the same set. Training and testing are repeated as above. The statements concerning set independence also apply here. Using two testing sets provides an indication of the spread to be expected in the classification rates.

Figure 12 shows the linear classifier results. The Fourier transform performs better by several percent. The spread in classification rates is smaller for the Fourier transform. Even larger differences appear using the quadratic classifier as seen in Fig. 13. The Fourier transform outperforms the Fourier-Mellin by 5 to 15%.

From these examples it appears that the Fourier-Mellin transform does not provide significantly improved classification to justify the additional computational expense required. Indeed, for the actual ship data, the Fourier-Mellin transform performs significantly poorer than the Fourier transform alone.

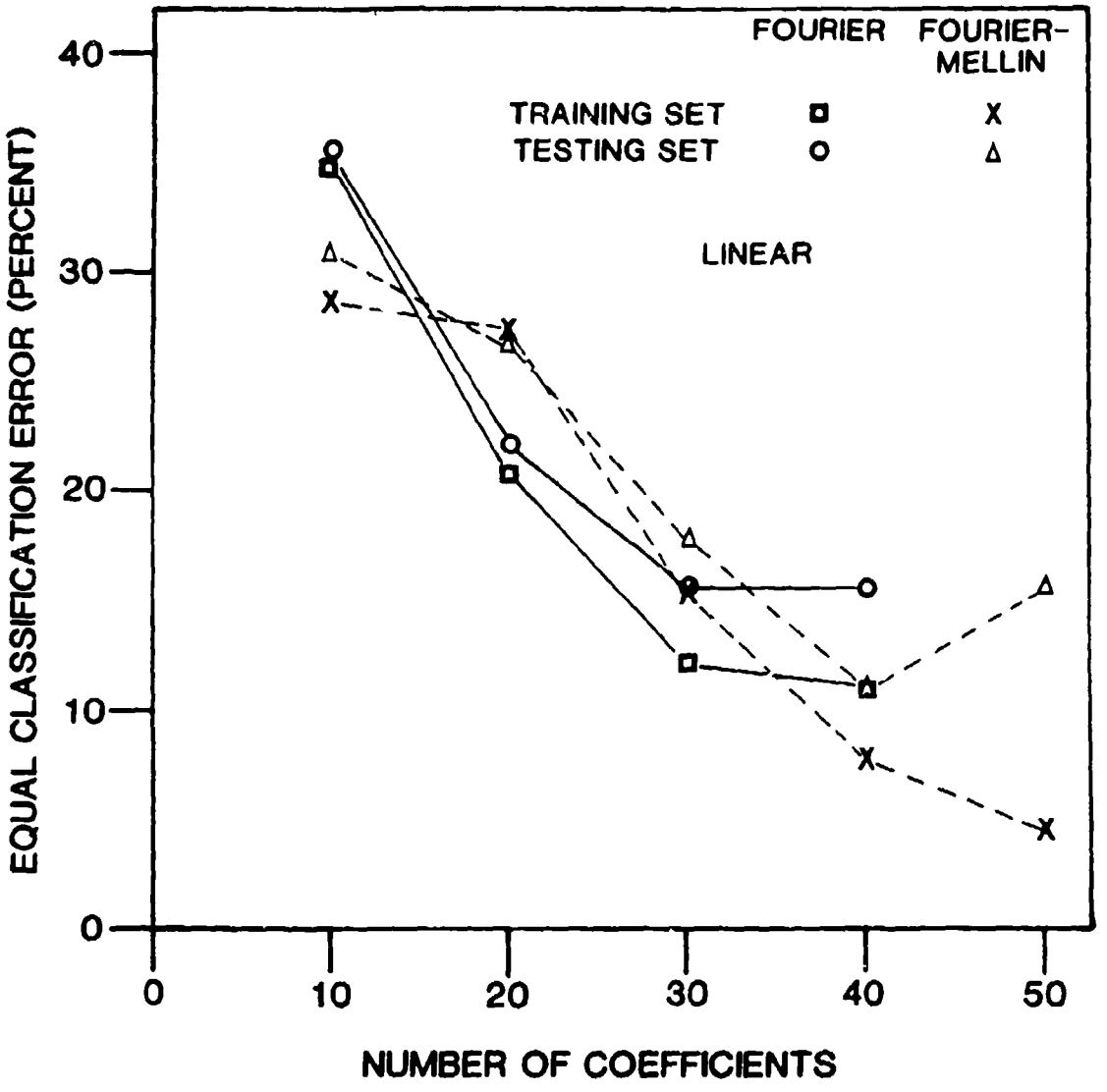


Fig. 10. Linear classifier results for simulated ship profiles

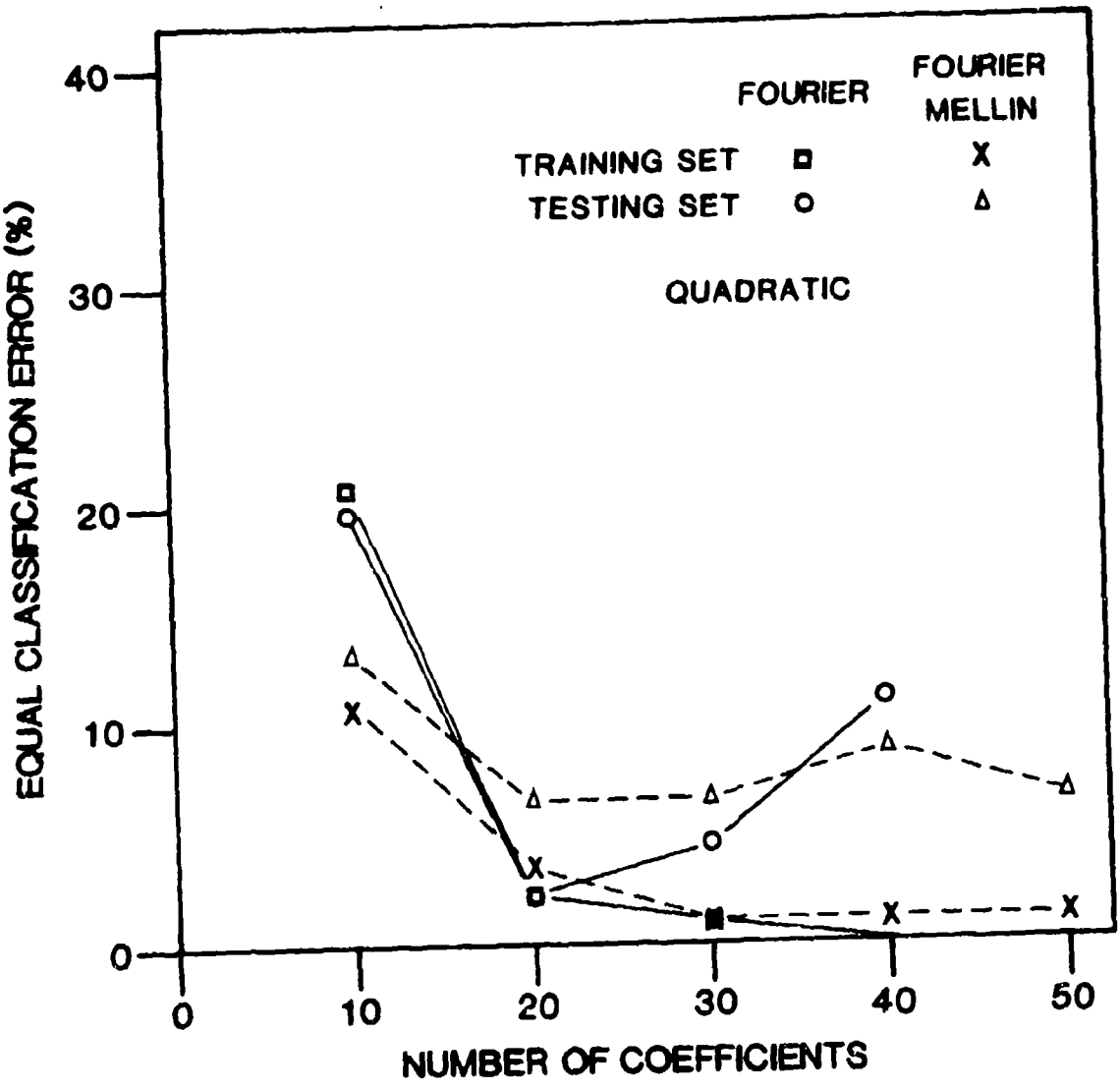


Fig. 11. Quadratic classifier results for simulated ship profiles

RST-5 (12)

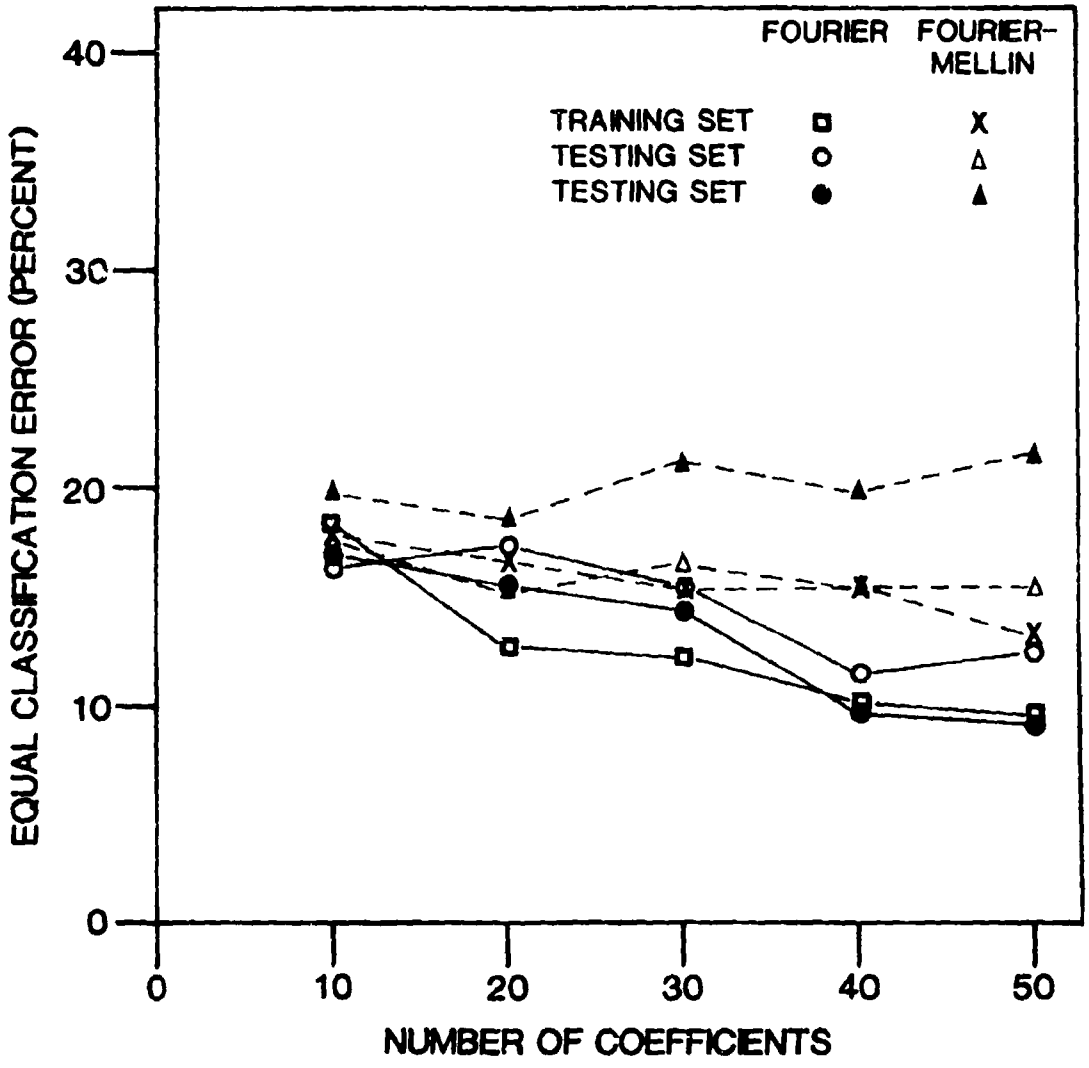


Fig. 12. Linear classifier results for measured ship profiles

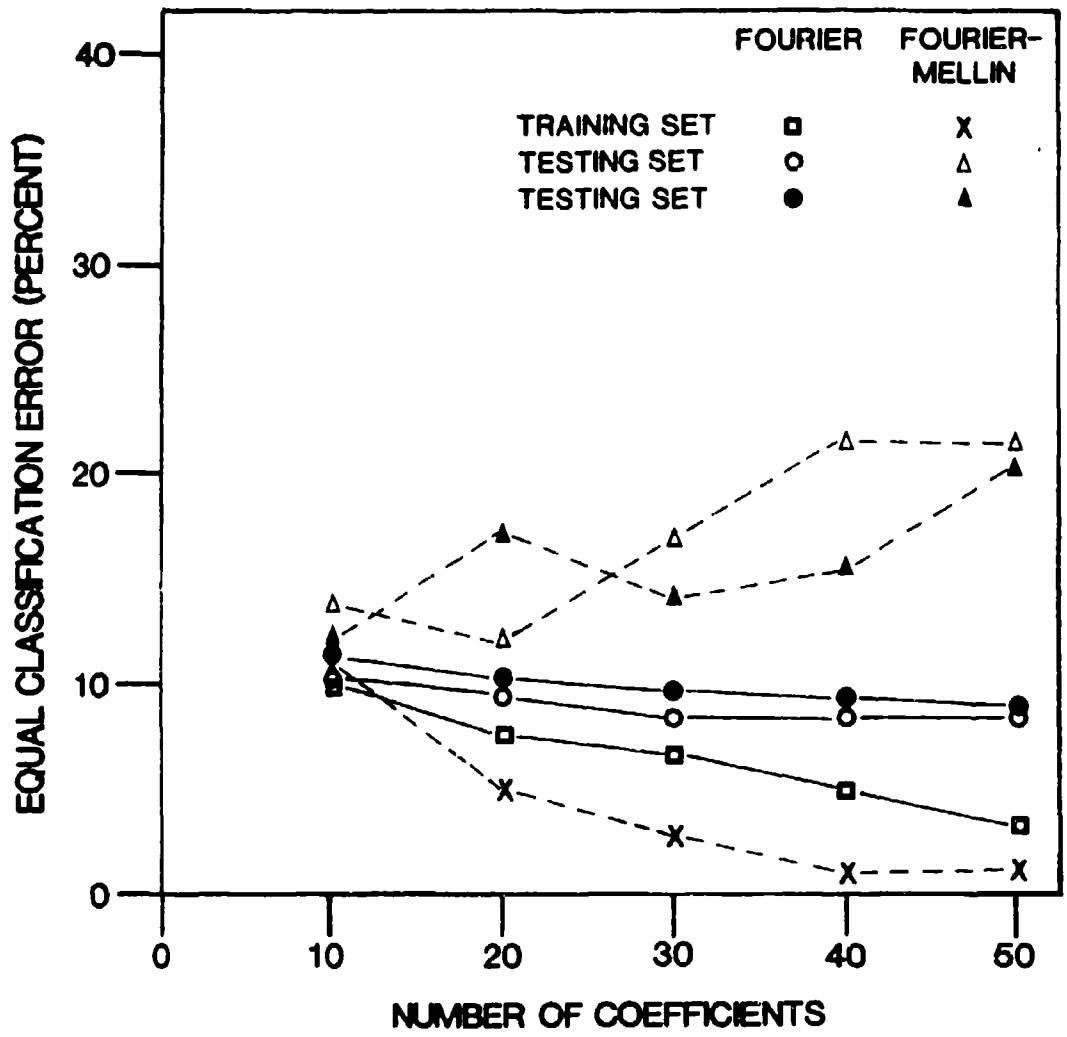


Fig. 13. Quadratic classifier results for measured ship profiles

## 7. SUMMARY AND CONCLUSIONS

This report summarizes the investigation into the Mellin transform and its possible use in pattern classification of radar ship profiles. The emphasis is on digital implementation and insight into the physical operation of the transform rather than its formal mathematical properties. A combination Fourier-Mellin transform invariant under both shift and scale operations is studied in the same manner.

A change of variable converts a Mellin into a Fourier transform but with a distorted input function. For discretely sampled functions the Fourier transform may be evaluated using the FFT algorithm. This requires resampling of the function, however, at nonuniform intervals via interpolation. Evaluation of the discrete Fourier transform is equivalent to numerically approximating an integral with an accuracy related to the sampling rate of the function.

Mellin and Fourier-Mellin transforms of test functions are shown. The scale invariance of the Mellin and the shift and scale invariance of the Fourier-Mellin transform are illustrated. The scale invariance exhibited is shown to be related to the sampling rate. Transforms of simulated radar ship profiles are presented. The profiles emphasize that changes in aspect are not equivalent to scaling of the target.

Neither Fourier nor Fourier-Mellin transforms are invariant to target aspect changes. The utility of each transform as a feature selector in ship classification is investigated by comparing classification performance. Linear and quadratic classifiers are applied to both simulated and actual radar ship profiles. In the cases tested, the Fourier-Mellin classification appears to be no better and possibly worse than Fourier classification.

The Fourier-Mellin transform can be potentially useful for problems involving shift and scale operations. Based upon the cases tested, the transform appears to be no more useful than the Fourier transform alone for automatic classification of radar ship profiles.

## REFERENCES


{1} R. N. Bracewell, The Fourier Transform and Its Applications, (McGraw-Hill, New York, 1978).

{2} I. N. Sneddon, The Use of Integral Transforms, (McGraw-Hill, New York, 1972).

{3} D. Casasent, and D. Psaltis, "New Optical Transforms for Pattern Recognition," Proc. IEEE 65, 77-84 (1977).

{4} P. Kellman, and J. W. Goodman, "Coherent Optical Implementation of 1-D Mellin Transforms," Appl. Opt. 16, 2609-2610 (1977).

{5} G. M. Robbins, and T. S. Huang, "Inverse Filtering for Linear Shift-Variant Imaging Systems," Proc. IEEE 60, 862-872 (1972).

{6} D. Casasent, and D. Psaltis, "Space-Bandwidth Product and Accuracy of the Optical Mellin Transform," Appl. Opt. 16, 1472 (1977).

{7} D. Casasent, and D. Psaltis, "Accuracy and Space Bandwidth in Space Variant Optical Correlators," Opt. Commun. 23, 209-212 (1977).

## GLOSSARY

| | |
|---|---|
| FFT | Fast Fourier Transform |
| LHS | Left-Hand Side |
| RCS | Radar Cross Section |
| RHS | Right-Hand Side |
| RLOS | Radar Line-of-Sight |

UNCLASSIFIED

SECURITY CLASSIFICATION OF THIS PAGE (When Data Entered)

| REPORT DOCUMENTATION PAGE | READ INSTRUCTIONS BEFORE COMPLETING FORM |
|---|---|
| 1. REPORT NUMBER: ESD-TR-80-197 | 2. GOVT ACCESSION NO.: AD-A093690 | 3. RECIPIENT'S CATALOG NUMBER |
| 4. TITLE (and Subtitle): The Shift and Scale Invariant Fourier-Mellin Transform for Radar Applications | 5. TYPE OF REPORT & PERIOD COVERED: Project Report |
| | 6. PERFORMING ORG. REPORT NUMBER: Project Report RST-5 |
| 7. AUTHOR(s): Lyle H. Johnson | 8. CONTRACT OR GRANT NUMBER(s): F19628-80-C-0002 |
| 9. PERFORMING ORGANIZATION NAME AND ADDRESS: Lincoln Laboratory, M.I.T.<br>P.O. Box 73<br>Lexington, MA 02173 | 10. PROGRAM ELEMENT, PROJECT, TASK AREA & WORK UNIT NUMBERS: Program Element No. 62712N |
| 11. CONTROLLING OFFICE NAME AND ADDRESS: Deputy Assistant Secretary of the Navy ($C^3$1)<br>Office of the Assistant Secretary of the Navy (RE&S)<br>Washington, DC 20350 | 12. REPORT DATE: 14 October 1980<br>13. NUMBER OF PAGES: 56 |
| 14. MONITORING AGENCY NAME & ADDRESS (if different from Controlling Office): Electronic Systems Division<br>Hanscom AFB<br>Bedford, MA 01731 | 15. SECURITY CLASS. (of this report): Unclassified<br>15a. DECLASSIFICATION DOWNGRADING SCHEDULE |

16. DISTRIBUTION STATEMENT (of this Report)

Approved for public release; distribution unlimited.

17. DISTRIBUTION STATEMENT (of the abstract entered in Block 20, if different from Report)

18. SUPPLEMENTARY NOTES

None

19. KEY WORDS (Continue on reverse side if necessary and identify by block number)

Mellin transform | radar ship profiles | Fast Fourier Transform (FFT)

20. ABSTRACT (Continue on reverse side if necessary and identify by block number)

Automatic classification of targets viewed by radar is complicated by variations in target aspect relative to the radar line-of-sight (RLOS). This report investigates the possibility of reducing the effects of target aspect by using the scale invariance of the Mellin transform. The properties of the Mellin transform are developed in analogy with the Fourier transform and illustrated using simple test functions and digitally implemented transforms. Simulated radar ship profiles demonstrate that a change in aspect is not equivalent to a change in target scale for realistic targets, however. Automatic classification results, for both simulated and actual radar ship profiles, confirm that using a combination Fourier-Mellin transform for feature selection appears at best comparable to the results obtained using the Fourier transform alone for feature selection.

DD FORM 1 JAN 73 1473 EDITION OF 1 NOV 65 IS OBSOLETE

UNCLASSIFIED

SECURITY CLASSIFICATION OF THIS PAGE (When Data Entered)